RSC Advances

PAPER

View Article Online
View Journal | View Issue

Cite this: *RSC Adv.*, 2024, **14**, 24910

Development and characterization of three-dimensional antibacterial nanocomposite sponges of chitosan, silver nanoparticles and halloysite nanotubes†

A. Hernández-Rangel, *[a] P. Silva-Bermudez,[c] A. Almaguer-Flores,[d] V. I. García,[d] R. Esparza, [e] G. Luna-Bárcenas*[b] and C. Velasquillo*[c]

In this work, we developed novel nanocomposite three-dimensional (3D) scaffolds composed of chitosan (CTS), halloysite nanotubes (HNTs) and silver nanoparticles (AgNPs) with enhanced antimicrobial activity and fibroblast cell compatibility for their potential use in wound dressing applications. A stock CTS–HNT solution was obtained by mixing water-dispersed HNTs with CTS aqueous-acid solution, and then, AgNPs, in different concentrations, were synthesized in the CTS–HNT solution *via* a CTS-mediated *in situ* reduction method. Finally, freeze-gelation was used to obtain CTS–HNT–AgNP 3D porous scaffolds (sponges). Morphology analysis showed that synthesized AgNPs were spherical with an average diameter of 11 nm. HNTs' presence did not affect the AgNPs morphology or size but improved the mechanical properties of the scaffolds, where CTS–HNT sponges exhibited a 5 times larger compression stress than bare-CTS sponges. AgNPs in the scaffolds further increased their mechanical strength in correlation to the AgNP concentration, and conferred them improved antibacterial activity against Gram-negative and Gram-positive bacteria, inhibiting the planktonic proliferation and adhesion of bacteria in a AgNP concentration depending on manner. *In vitro* cell viability and immunofluorescence assays exhibited that human fibroblast (HF) culture was supported by the sponges, where HF retained their phenotype upon culture on the sponges. Present CTS–HNT–AgNP sponges showed promising mechanical, antibacterial and cytocompatibility properties to be used as potential scaffolds for wound dressing applications.

Received 11th June 2024
Accepted 30th July 2024

DOI: 10.1039/d4ra04274c

rsc.li/rsc-advances

1. Introduction

The skin is the largest organ in the human body and constitutes its main defensive barrier against massive fluid loss, mechanical damage, and pathogen microorganism invasion. Upon mild injuries, the skin can self-regenerate. However, when damage extends to a large surface area and beyond the skin top layer, damaging the dermis, hypodermis, or even muscle and bone as in the case of severe second-deep or third-degree burns, or when the healing process is somehow disrupted and proceeds in a non-orderly and non-timely manner as in the case of diabetic foot ulcers, then specialized treatment is required to achieve proper wound healing. Treatment of chronic and severe acute wounds represents a significant burden for health care systems around the world.[1] Typically, wound management involves two main steps: cleansing and dressing, where dressings are ideally expected to control fluid loss, transfer exudates away from the wound site, prevent infection and promote healing. Despite numerous efforts in this field, designing the scaffold with the ideal structural and biological properties for wound dressing remains elusive.[2] Ideally, the scaffold would be expected to present a three-dimensional (3D) structure, large porosity with highly uniform pores, adequate mechanical properties, controlled degradation rate, antibacterial activity, biocompatibility and biofunctionality.[3,4]

Chitosan (CTS) is particularly interesting for developing scaffolds for wound dressing applications,[5–7] because it is biocompatible and biodegradable, presents a chemical structure similar to that of glycosaminoglycans in the dermis extracellular matrix (ECM),[8,9] displays antibacterial properties, promotes cell adhesion, increases collagen fiber deposition and enhances formation of granulation tissue, all contributing to

[a]*Instituto Politécnico Nacional, ESIQIE, Av. IPN S/N Zacatenco, Mexico City, 07738, Mexico. E-mail: adhernandezra@ipn.mx*

[b]*Centro de Investigación y de Estudios Avanzados del IPN, 76230, Querétaro, Mexico. E-mail: glunascf@yahoo.com*

[c]*Unidad de Ingeniería de Tejidos, Terapia Celular y Medicina Regenerativa, Instituto Nacional de Rehabilitación Luis Guillermo Ibarra Ibarra, 14389, Ciudad de México, Mexico. E-mail: mvelasquillo@inr.gob.mx*

[d]*División de Estudios de Posgrado e Investigación, Facultad de Odontología, Universidad Nacional Autónoma de México, 04510, Ciudad de México, Mexico*

[e]*Centro de Física Aplicada y Tecnología Avanzada, Universidad Nacional Autónoma de México, Boulevard Juriquilla 3001, Santiago de Querétaro 76230, Mexico*

† Electronic supplementary information (ESI) available. See DOI: https://doi.org/10.1039/d4ra04274c

promote wound healing.[8,10–13] Moreover, the amino and hydroxyl functional groups in CTS chemical structure enable its interaction with other compounds, allowing the formation of CTS-based composite materials with improved properties. Numerous studies have reported the development of CTS scaffolds for different biomedical applications; however, scaffolds obtained from pristine CTS normally possess poor mechanical properties and have proved challenging achievement of uniform porous structures.[13–16] Therefore, different strategies have been explored to obtain CTS-based scaffolds with desirable 3D structures and improved mechanical properties. Among the different strategies explored, integration of nanofillers into CTS matrices has shown to significantly enhance the mechanical properties of the scaffolds as well as yielding highly homogeneous porous structures. A variety of materials such as carbon nanotubes,[17,18] graphene oxide[19–21] and clays[22–27] have been studied as nanofillers for this purpose.

Halloysite nanotubes (HNTs) have gained attention as efficient reinforcement nanofillers, mainly because of their biocompatibility, ease of dispersion, high availability and low cost.[28–32] HNTs are aluminosilicate clays from the kaolin group with empirical formula $Al_2Si_2O_5(OH)_4 \cdot nH_2O$,[33,34] and are mainly found as hollow cylinders of 50–2000 nm average length and internal and external diameters of 10–70 and 20–200 nm, respectively.[29,31] Outer and inner surfaces of HNTs are mostly composed of siloxanes (Si–O–Si) and aluminol (Al–OH) groups, respectively, and hence, they are negatively and positively charged, correspondingly.[34] Appropriate integration of HNTs within CTS matrices can be achieved in acidic medium through strong electrostatic interactions between the positively charged amino groups of CTS and the negatively charged outer surface of HNTs.[35,36] Liu *et al.* prepared CTS–HNTs sponges demonstrating that HNTs incorporation enhanced the mechanical properties of the sponges, and improved fibroblasts attachment, and hemostatic and wound healing properties.[37,38] Similar results have been published by other authors for CTS composites added with HNTs, showing improved fibroblasts proliferation and migration *in vitro*, and enhanced wound reepithelization and reorganization *in vivo*,[22,32,39,40] further supporting the potential of CTS–HNTs nanocomposites as potential scaffolds for wound dressing applications.

Previous reports have demonstrated that addition of metallic nanoparticles (NPs) into polymer matrices can also enhances their mechanical properties,[41,42] where the addition of antibacterial metallic NPs can incorporate the further advantage of developing not only reinforced but also antibacterial nanocomposites. It is important to emphasize that preventing bacterial infection is crucial for successful wound healing, since infection is one of the main complications hampering appropriate wound healing during treatment of acute-severe or chronic wounds.[43,44] Silver nanoparticles (AgNPs) have been widely studied and are well-known for their antimicrobial action against yeast,[45,46] fungus[47,48] and bacteria.[49,50] CTS–AgNPs films obtained by $AgNO_3$ *in situ* reduction, using CTS as the reducing and stabilizing agent, displayed enhanced antibacterial activity against *Staphylococcus aureus* and *Pseudomonas aeruginosa* in comparison to CTS films, with low AgNPs concentration being permissive for fibroblasts culture on the films, evidencing the potential of CTS–AgNPs films as antibacterial scaffolds for wound dressing applications.[51,52] One of the main concerns when using antibacterial metallic NPs for biomedical applications is the undesirable uncontrolled release of the NPs into the biological medium, that might cause significant cytotoxic effects,[53,54] as well as the agglomeration of the NPs that might decrease their antibacterial activity being this a highly surface-dependent on phenomenon.[55,56] In this sense, HNTs, in addition to their use as mechanical reinforcement fillers for polymeric matrices, have been successfully used for AgNPs immobilization[57,58] in a wide range of fields such as catalysis,[59,60] biosensing,[61,62] surface enhanced Raman scattering,[63] filtration[64–66] and antibacterial materials development,[67–72] improving the dispersibility and stability of the AgNPs, and decreasing their leaching, while maintaining their antibacterial activity.[73]

Herein, we combine the biological advantages of CTS, the antibacterial properties of AgNPs, and the advantageous nanofiller-reinforcement and NPs-stabilization characteristics of HNTs, reporting a facile green synthesis process to obtain CTS–HNT–AgNP nanocomposite sponges with promising antibacterial, structural, mechanical and non-cytotoxic properties to be used as potential scaffolds for wound dressing applications. CTS–HNT–AgNP sponges with different AgNPs concentrations were obtained by *in situ* reduction of $AgNO_3$ in CTS–HNTs solution, followed by frozen-gelation. The physical, chemical and mechanical properties of the sponges were characterized, their antibacterial activity was tested against Gram-negative (*Escherichia coli* and *P. aeruginosa*) and Gram-positive (*Staphylococcus epidermidis* and *S. aureus*) bacteria strains, and human dermal fibroblasts (HF) were used as a model to explore the sponges' cytocompatibility.

2. Materials and methods

2.1. Materials and reagents

CTS (M_w = 300 kDa and 82% deacetylation), HNTs ($H_4Al_2O_9Si_2 \cdot 2H_2O$), $AgNO_3$ and glacial acetic acid were purchased from Sigma-Aldrich; all reagents were analytical grade and were used as received. The degradation rate tests were performed using Egg Hen lysozyme (Sigma-Aldrich) and Phosphate Buffer Saline solution (PBS, 1X; Gibco). For antibacterial experiments, enriched Trypticase Soy Broth (TSB), menadione and hemin were purchased from Sigma-Aldrich. Percentage of viable bacterial cells adhered to sponge samples was evaluated with MTT (3-(4,5-dimethylthiazol-2-yl)-2,5-diphenyltetrazolium bromide; Sigma-Aldrich). For tissue processing to isolate fibroblast cells and for fibroblasts culture, phosphate buffer solution (PBS, pH = 7.4), dispase II, type I collagenase, Dulbecco's Modified Eagle Medium (DMEM:F12), Fetal Bovine Serum (FBS), antibiotic/antimycotic (penicillin/streptomycin) and trypsin-EDTA were all purchased from Gibco. Cell viability on the sponges was assessed using the live/dead (green/red) calcein-AM/ethidium homodimer fluorescent kit (LIVE/DEAD® Viability/Cytotoxicity Kit for mammalian cell; Molecular Probes, Invitrogen) and Hank's Balanced Salt Solution (Gibco).

Finally, for immunofluorescence assays, Triton and bovine serum albumin were purchased from Sigma-Aldrich, and rabbit primary anti-human antibody to α-SMA (Abcam, ab5694) and goat anti-rabbit FITC secondary fluorescent antibody (Abcam, ab6717) were used.

2.2. Synthesis of CTS–HNT–AgNP nanocomposite sponges

A CTS stock solution was prepared by dissolving CTS (2% w/v) in 1% aqueous acetic acid under vigorous stirring until a clear solution was obtained. For the CTS–HNTs stock solution, HNTs dispersed in deionized water (4% w/v) were mixed with the CTS stock solution in a 1 : 2 (v/v) ratio. Then, CTS–AgNPs and CTS–HNTs–AgNPs nanocomposite colloidal suspensions were prepared as previously reported,[61] using $AgNO_3$ as the AgNPs precursor and CTS as the reducing and stabilizing agent. Briefly, aqueous 0.010, 0.025, 0.050 and 0.100 M $AgNO_3$ solutions were prepared with deionized water. Then, 160 μL of each $AgNO_3$ solution was independently added to 20 mL of CTS or CTS–HNTs stock solution and kept under magnetic stirring at 95 °C for 8 h to obtain CTS–AgNPs or CTS–HNTs–AgNPs nanocomposite colloidal suspensions, respectively. Then, CTS–AgNP and CTS–HNT–AgNP porous 3D nanocomposite scaffolds (sponges) were produced by frozen-gelation according to Ho *et al.*[74] Briefly, CTS–AgNPs and CTS–HNTs–AgNPs nanocomposite colloidal suspensions were independently poured into Petri dishes and frozen at −20 °C for 12 h. Frozen nanocomposites were immersed in 1 M ethanolic NaOH solution and kept at −20 °C for 3 days. Gelled nanocomposites were washed thoroughly with MilliQ® water at room temperature (RT), and the sponges obtained were left to dry at RT and stored at normal ambient conditions for further use. Pristine CTS and CTS–HNT sponges were also obtained as controls. Sponges samples were named as indicated in Table 1.

2.3. Physical–chemical characterization of the nanocomposite sponges

CTS–AgNP and CTS–HNT–AgNP nanocomposite colloidal suspensions were analyzed by Transmission Electron Microscopy (TEM; JEOL JSM-1010). Samples for TEM analysis were prepared by independently depositing a drop of CTS–AgNP and CTS–HNTs–AgNPs colloidal suspensions on carbon-coated copper grids and allowing them to dry at RT. TEM micrographs were acquired at 80 kV and analyzed with the Image J® software to determine distribution and average size of AgNPs.

Porous morphology of the sponges was corroborated by Scanning Electron Microscopy (SEM; Hitachi SU8230) operated at 6 kV; dry sponges samples were Au-coated before SEM analysis.

Silver concentration in the sponges was determined by Inductively Coupled Plasma-Optical Emission Spectroscopy (ICP-OES; Ultima-2, Horiba). Sponges samples were independently digested in a microwave (multi-wave PRO, Anton Paar) with 7 vol% HNO_3 aqueous solution. Then, silver concentration was measured by ICP-OES with silver detection low limit of 0.6 μg L^{-1}.

Fourier Transform Infrared Spectroscopy (FTIR; PerkinElmer spectrophotometer coupled with an ATR accessory) was used to study the chemical interactions in the sponges. FTIR spectra were acquired with 24 scans and 4 cm^{-1} resolution in the range of 4000–650 cm^{-1} from dry sponges samples.

Sponges water uptake capacity was measured by weighing dry samples of the sponges (W_1), and then, independently immersing them into phosphate buffer solution (PBS, pH = 7.4; Gibco) at 37 °C. At 0.5, 1, 3, 6 and 24 h of immersion, samples were taken out, water excess was removed with filter paper and samples weight was measured again (W_2). Experiments were independently performed by triplicate for each sponges group. Sponges water uptake in percentage (swelling %) was calculated according to eqn (1)

$$\text{Swelling}(\%) = \frac{W_2 - W_1}{W_1} \times 100 \quad (1)$$

To measure the degradation of the sponges over time, dry samples of the sponges were independently weighed (W_0) and incubated in PBS containing 5 mg mL^{-1} of Egg Hen lysozyme. Samples were incubated at 37 °C for 4, 7, 14 and 21 days under orbital shaking. At each time interval, samples were taken out, thoroughly washed with MilliQ® water, dried out and weighed (W_1). Weight loss percentage (weightloss %) was calculated following eqn (2); all experiments were performed by triplicate.

$$\text{Weightloss}(\%) = \frac{W_0 - W_1}{W_0} \times 100 \quad (2)$$

Porosity of the sponges in percentage (porosity %) was measured by the liquid displacement method.[75] The volume and weight of cylindrical dry sponges samples were measured and noted as V and W_1, respectively. Then, samples were immersed in absolute ethanol until saturation and weighed again. Samples weight after ethanol immersion was noted as W_2, and used in eqn (3) to calculate the porosity % of the sponges.

$$\text{Porosity}(\%) = \frac{W_2 - W_1}{\rho V} \times 100 \quad (3)$$

where ρ corresponds to the density of absolute ethanol.

Table 1 Synthesized CTS–AgNPs and CTS–HNTs–AgNPs sponges

Sponges nomenclature		
CTS–AgNPs	CTS–HNTs–AgNPs	$AgNO_3$ concentration[a] (M)
p-CTS	CTS–HNT	0.00
01-CTS–AgNP	01-CTS–HNT–AgNP	0.01
02-CTS–AgNP	02-CTS–HNT–AgNP	0.02
05-CTS–AgNP	05-CTS–HNT–AgNP	0.05
10-CTS–AgNP	10-CTS–HNT–AgNP	0.10

[a] $AgNO_3$ concentration in the silver-precursor aqueous solution used to synthesize the CTS–AgNP and CTS–HNT–AgNP nanocomposite colloidal suspensions that were gel-frozen to obtain the different nanocomposite sponges.

To evaluate silver release from the sponges in aqueous media, dry samples (weighing 0.230 g) of the sponges were independently immersed in 30 mL of PBS and incubated at 37 °C under orbital shaking. Incubation supernatants were collected every 24 h and replaced with the same amount of fresh PBS. Collected supernatants were digested as previously described for ICP-OES measurements, and silver concentration was quantified by ICP-OES with a lower limit silver detection of 0.6 μg L^{-1}. Data are presented as the time-cumulative silver release at each measurement time.

Compression tests were performed to characterize the mechanical properties of the sponges. Tests were carried out in a Texture Analyzer (TA-TX2 plus) at RT. Sponges samples used for mechanical testing were fully hydrated and cylindrical in shape with 4 mm diameter and 3 mm thickness at full hydration. Crosshead speed during mechanical testing was 0.01 mm s^{-1} and samples were compressed to 90% strain. The elastic compressive modulus (E) of the sponges was calculated, and it is reported along with the compressive stress at 80% strain. Three independent experiments were performed for each sponges group.

2.4. Antibacterial activity of the nanocomposite sponges

Four bacteria strains, *S. epidermidis*, *E. coli*, *S. aureus* and *P. aeruginosa* (ATCC 14990, 33780, 25923 and 43 636, respectively), representative of common nosocomial wound- and burn-related infections were used to test the antimicrobial activity of the sponges. Bacterial strains were chosen as representative of Gram-negative (*E. coli* and *P. aeruginosa*) and Gram-positive (*S. epidermidis* and *S. aureus*) bacteria. Antibacterial activity of the sponges was independently studied against each bacterial strain according to the following procedure. UV-sterilized (λ = 254 nm) and hydrated circle-shaped (8 mm in diameter) sponge samples were individually placed in 24-well tissue culture plates. The growth of bacteria was harvested from agar plates and suspended in enriched Trypticase Soy Broth added with 0.3 μg mL^{-1} menadione and 5 μg mL^{-1} hemin. Optical density of bacterial solution was adjusted to 1 at 600 nm in a spectrophotometer to obtain a stock bacterial suspension with $\approx 1 \times 10^8$ bacterial cells per mL. Adequate amounts of stock bacterial suspension were independently added to wells containing the sponge samples to a final concentration of 1×10^6 bacterial cells per mL in enriched TSB medium. Samples were incubated for 24 h at 36 °C in an orbital shaker incubator. Antimicrobial activity of the sponges was characterized at 24 h of culture. Turbidity measurements of culture medium were performed to evaluate the inhibition of bacterial planktonic growth exerted by the sponges. MTT assays were performed on the bacteria-incubated sponges samples to evaluate the inhibition of bacterial attachment and growth on the sponges, as the first natural steps occurring before biofilm formation.

For turbidity measurements, absorbance of the incubation medium, after 24 h of bacteria incubation in presence of the sponges, was read at 595 nm in a spectrophotometer (Filter Max F5). Absorbance reads of incubation medium from bacteria incubated in tissue culture well plates with no sponges were considered as negative antibacterial controls (100% planktonic bacterial growth). Data are presented as percentage of planktonic bacterial growth, in comparison to negative antibacterial control, according to eqn (4).

$$\text{Planktonic bacterial growth}(\%) = \frac{\text{Abs} - \text{Absp}}{\text{Absn} - \text{Absp}} \times 100; \quad (4)$$

where Abs is the absorbance read of bacteria incubation medium in presence of sponges samples, Absp is the absorbance read from fresh incubation medium (basal absorbance read), and Absn is the absorbance read from bacteria incubation medium in presence of no sponges (negative antibacterial control).

For MTT assays (which can be used to denote dehydrogenase activity of living bacterial cells), 24 h bacteria-incubated sponge samples were thoroughly washed with fresh TSB medium to detach loosely attached bacteria. Then, the sponge samples were independently placed on clean 24-well tissue culture plates and incubated with MTT : TSB (1 : 10) solution at 37 °C for 3 h. After MTT incubation, bacteria-metabolized formazan crystals were solubilized in 2-propanol : DMSO (1 : 1) solution and absorbance of formazan crystals dissolution was read at 570 nm in a spectrophotometer (FilterMax F5). Absorbance reads of bacteria-incubated p-CTS and CTS–HNT sponge samples (that is, sponge samples with no AgNPs) were considered as controls to evaluate the effect of the AgNPs concentration on the inhibition of bacterial attachment and growth on the sponges. Absorbance reads of bacteria incubated (attached) in tissue culture well plates with no sponges were considered as negative controls (100% bacterial attachment, that is, no inhibition on bacterial attachment and growth). Data are presented as percentage of viable bacterial cell attached to the sponges, calculated according to eqn (5).

$$\text{Viable attached bacteria}(\%) = \frac{\text{Abs} - \text{Absp}}{\text{Absn} - \text{Absnp}} \times 100; \quad (5)$$

where Abs is the absorbance read from bacteria attached to the sponge samples, Absp is the absorbance read of sponges incubated with no bacteria (to discard any possible non-specific interaction of MTT with the sponges components), Absn is the absorbance read of bacteria attached on tissue culture well plates incubated with no sponges samples (negative antibacterial control; no inhibition of bacterial attachment and growth inhibition) and Absnp is the absorbance read of isopropanol:DMSO solution (basal absorbance read).

The agar diffusion test was used to assess the bacterial response to the possible silver release (and diffusion) from the sponges, which might occur upon a potential application of the sponges as scaffolds for wound dressings. Agar medium can be seen as a model of the humid ambient present in wound beds during the first stages of wound healing. Petri dishes with Mueller–Hinton agar were uniformly inoculated with 1 mL of stock bacterial suspension. Then, UV-sterilized, fully hydrated, circle-shaped (8 mm in diameter) sponge samples were placed on the inoculated Petri dishes and incubated for 24 h at 35 °C. Independent p-CTS and CTS–HNT samples impregnated with chlorhexidine gluconate antiseptic were used as positive

antibacterial controls. After 24 h of incubation, disc inhibition zones were measured and compared.

All antibacterial experiments were repeated twice by triplicate pear each different sponge group and bacteria strain studied.

2.5. Cytocompatibility evaluation of the nanocomposite sponges

Human dermal fibroblasts were isolated from foreskin biopsies discarded from circumcision surgeries of healthy pediatric patients. Parents of all subjects responded to an Informed Consent approved by the Institutional Committee on Human Research of the Instituto Nacional de Rehabilitación Luis Guillermo Ibarra Ibarra (Mexico, Project registry INR-11/12). HF isolation was performed as previously reported.[76] Briefly, foreskin biopsies were washed with 10% v/v antibiotic-antimycotic in PBS, mechanically fragmented, and treated with dispase II. Then, the epidermis was discarded, and the dermis was enzymatically digested. HF were recovered by centrifugation, plated in culture flasks with Dulbecco's Modified Eagle Medium supplemented with 10% v/v fetal bovine serum and 1% v/v antibiotic–antimycotic (anti:anti), and incubated at 37 °C in a 5% CO_2 atmosphere; medium was changed every 2 days. For subcultures, confluent HF monolayers were treated with 0.05% v/v trypsin-EDTA (0.25%) in PBS, collected, resuspended and plated in culture flasks with fresh culture medium. Cells were expanded until passage 3–4 when were used for *in vitro* cytocompatibility testing of the sponges.

To evaluate the cytocompatibility of the sponges, UV-sterilized, fully hydrated sponge samples were independently placed in 48-well tissue culture plates and seeded with HF in a drop-seeding technique to a cell density of 1.6×10^6 cells per cm^3. Samples were incubated for 2 h at 37 °C in 5% CO_2 atmosphere, and then culture medium was added to fully cover the samples, which were placed back in the incubator. Cell viability on the sponges was directly assessed at 8 days of culture using a live/dead (green/red) calcein-AM/ethidium homodimer fluorescent kit assay. Cells-cultured sponges were incubated with the LIVE/DEAD® kit assay according to the manufacturer guidelines, rinsed twice with PBS and immediately visualized by Confocal Microscopy (LSM 780 Carl Zeiss). Images were processed with the AxioVision® software.

Viability of cells on the sponges was also indirectly assessed by the MTT assay, which indicates the active mitochondrial activity of living cells. At 2 and 8 days of culture, independent cell-cultured sponge samples were washed and incubated with MTT : DMEM-F12 (1 : 10) solution for 3 h at 37 °C. After MTT incubation, medium was removed, and cell-metabolized formazan crystals were solubilized in DMSO : 2-propanol (1 : 1). Absorbance of formazan crystals dissolution was measured at 620 nm in a spectrophotometric microplate reader (FilterMax F5).

Immunofluorescence assays against alpha-Smooth Muscle Actin (α-SMA) were performed on HF cultured on the sponge groups that showed the highest cell viability by MTT assay (that is, p-CTS, CTS–HNT, 01-CTS–AgNP, 02-CTS–AgNP, 01-CTS–HNT–AgNP and 02-CTS–HNT–AgNP). Sponge samples were seeded with cells following the same procedure as described for HF seeding on the sponge samples intended for live/dead or MTT assays. Cell-seeded sponge samples were incubated for 8 days at 37 °C and 5% CO_2 atmosphere; culture medium was changed every 2 days. Then, samples were fixed with 2% PFA, rinsed with PBS, permeabilized with 0.3% Triton™ X-100 and blocked with 1% bovine serum albumin. Fixed samples were incubated overnight at 4 °C with primary antibody to α-SMA (rabbit primary anti-human antibody; 1 : 1000). After incubation, primary antibody was removed, and samples were incubated at 37 °C for 2 h with secondary fluorescent antibody (goat anti-rabbit FITC; 1 : 400). Finally, samples were rinsed, cell nuclei counterstained with ethidium homodimer and samples were visualized by Confocal Microscopy (LSM 780 Carl Zeiss).

All biocompatibility experiments were performed by triplicate for each sponges group studied.

2.6. Statistical analysis

Quantitative results are presented as mean ± standard error of the mean. For statistical significance, data were analyzed using the analysis of variance (one-way ANOVA) followed by Bonferroni's post-test for multiple comparisons. Significant differences indicated were set at $P < 0.05$.

3. Results

3.1. Physical–chemical characterization

Fig. 1 shows the macroscopic appearance of the synthesized CTS–AgNP and CTS–HNT–AgNP nanocomposites as colloidal suspensions, and after gelation process as sponges in their dry and fully hydrated states.

As complementary part of the nanocomposites characterization, pristine HNTs dispersed in ethanol were also analyzed by TEM; Fig. S1 (ESI)† show the representative micrographs from which it can be corroborated the tubular morphology of the HNTs with length, outer and inner diameter in the ranges of 200–600 nm, 70–100 nm and 40–50 nm, respectively.

CTS–AgNP and CTS–HNT–AgNP nanocomposites as colloidal suspensions before gelation were analyzed by TEM, and representative TEM micrographs, along with histograms of the AgNPs average size distribution are presented in Fig. 2. AgNPs in CTS–AgNP nanocomposites were well dispersed into the CTS matrix, showing a spherical shape with average diameter of 17 nm for all CTS–AgNP nanocomposites, but 01-CTS–AgNP which exhibited a larger AgNPs average size of 36 nm. The presence of the HNTs in the nanocomposites did not affect the shape of the AgNPs synthesized; however, AgNPs average size for CTS–HNT–AgNP nanocomposites decreased in comparison to that of the corresponding CTS–AgNP nanocomposites; Fig. 2. For CTS–HNT–AgNP nanocomposites, AgNPs average size decreased as AgNPs concentration increased, AgNPs average size was 18, 12, 7 and 4 nm for 01-CTS–HNT–AgNP, 02-CTS–HNT–AgNP, 05-CTS–HNT–AgNP and 10-CTS–HNT–AgNP, respectively. It is important to mention that AgNPs in CTS–HNT–AgNP nanocomposites were mainly

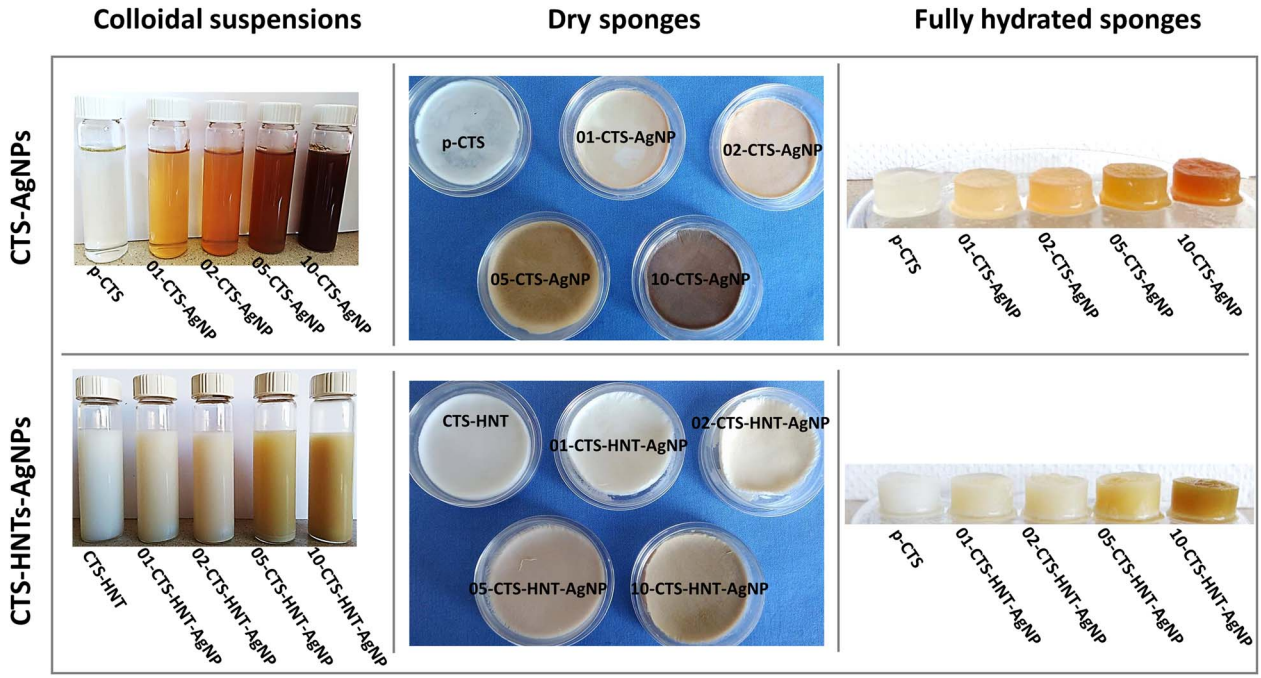

Fig. 1 Representative photographs of the macroscopic appearance of the synthesized CTS/AgNps and CTS/HNTs/AgNPs nanocomposites as colloidal suspensions, after the gelation process as sponges in their dry state, and after full hydration of the sponges.

around the external surface of the HNTs. In general, AgNPs around HNTs were smaller than those within the CTS matrix away from the HNTs surface.

The morphology of the sponges in their dry state was analyzed by SEM, and representative micrographs are shown in Fig. 3. p-CTS sponges presented a highly porous structure with average porosity of 87%, and porous that seemed to be interconnected presenting an average pore sizes of 80 μm; Fig. 4A and C. Addition of HNTs to the CTS matrix (CTS–HNT sponge) had no significant effect on neither the sponge pore size nor its porosity; Fig. 4B and D. Nevertheless, CTS–HNT sponges displayed a more homogenous and less-collapsed porous structure with better defined and more open pore walls than p-CTS; Fig. 3. AgNPs incorporation (CTS–AgNP and

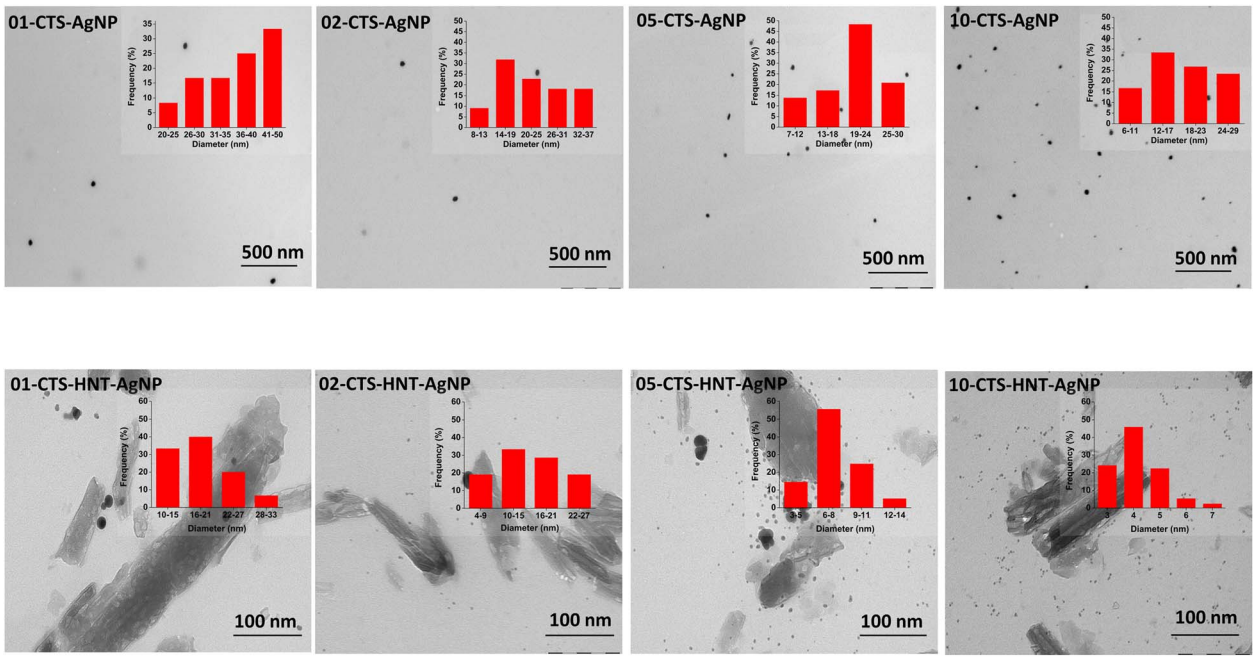

Fig. 2 Representative tem micrographs of the synthesized CTS/AgNPs and CTS/HNT/AgNPs nanocomposites as colloidal suspensions.

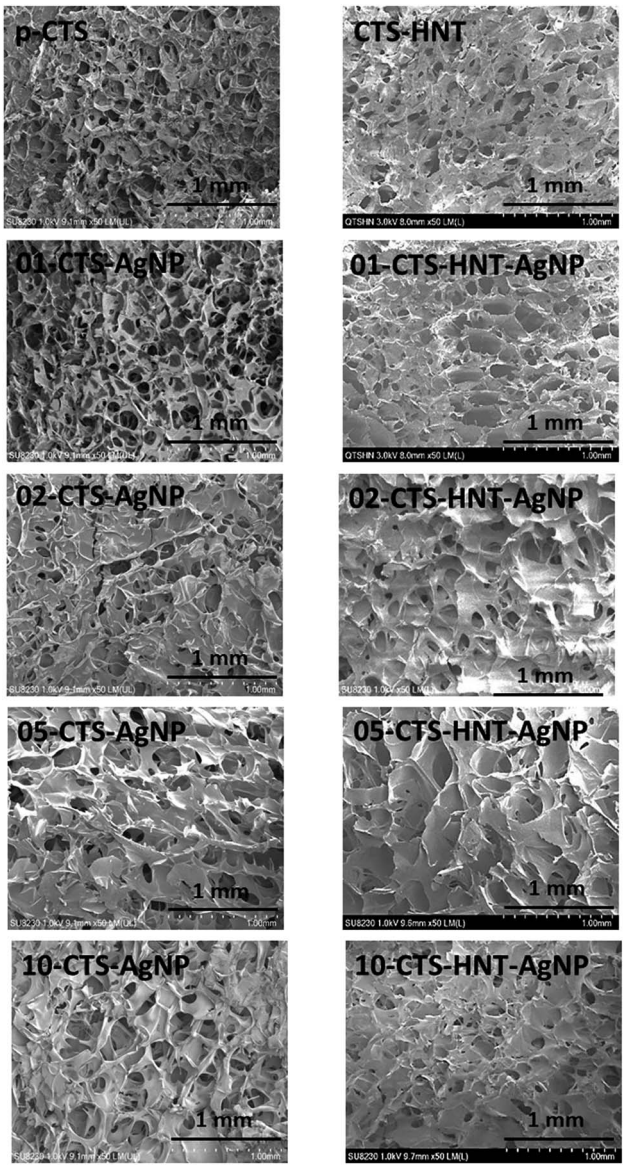

Fig. 3 Representative SEM images of the CTS/AgNPs and CTS/HNT/AgNPs sponges.

CTS–HNT–AgNP sponges) did not significantly affect the sponges average pore size in comparison to p-CTS or CTS–HNT, respectively; Fig. 4A and B. Nevertheless, porosity of the sponges decreased by ≈12% (Fig. 4C and D) for AgNPs-containing sponges in comparison to their corresponding sponges with no AgNPs, either p-CTS or CTS–HNT.

Silver content (wt%) in the sponges is summarized in Table 2. Silver content in the sponges increased as silver precursor concentration in the nanocomposite colloidal suspensions increased. However, increment in silver content, in wt% terms, was higher for CTS–AgNP sponges than that of their corresponding CTS–HNT–AgNP sponges, that is, 01-CTS–AgNP *vs.* 01-CTS–HNT–AgNP, 02-CTS–AgNP *vs.* 02-CTS–HNT–AgNP, *etc.*

Chemical interactions in the sponges were explored by FTIR spectroscopy and corresponding spectra, along with the IR spectrum of pristine HNTs, are shown in Fig. 5. p-CTS sponges exhibited clear IR bands at 3342 cm^{-1} (overlapped –OH and –NH stretching vibrations), 1650 cm^{-1} (amide I band), and 1590 cm^{-1} (in-plane $-NH_2$ bending vibration), in agreement with previous reports for CTS.[77] Pristine HNTs exhibited characteristic IR bands at 3695 and 3621 cm^{-1} corresponding to the –OH stretching of inner hydroxyl groups, and at 1118 and 1031 cm^{-1} assigned to Si–O stretching vibrations.[77] CTS–HNT sponges exhibited clear IR bands at 3695, 3621, 1118 and 1031 cm^{-1} corresponding to the characteristic IR bands of HNTs, in addition to the typical IR bands of CTS at 3342, 1650 and 1590 cm^{-1}; Fig. 5A.

In general, the same IR bands were observed for AgNPs-containing sponges as those for their corresponding sponges with no AgNPs, either for p-CTS- or CTS–HNT-based sponges; Fig. 5B and C. Nevertheless, a slight shifting of the IR bands associated to the amide I (CTS), NH_2 bending (CTS) and Si–O stretching (HNTs) vibrations can be noticed; Fig. 5D–F. When comparing the IR spectrum of p-CTS with those of the CTS–AgNP sponges (Fig. 5D), and the IR spectrum of CTS–HNT with those of the CTS–HNTs–AgNPs sponges (Fig. 5E) a slight upshift of the bands associated with the amide I (from 1650 to 1652 cm^{-1}) and NH_2 bending (from 1586 to 1590 cm^{-1}) vibrations can be observed for the AgNPs-containing sponges. In addition, upon AgNPs incorporation into the CTS–HNT based sponges (CTS–HNTs–AgNPs), the bands associated with the stretching of the Si–O groups in HNTs were downshifted (1114 and 1027 cm^{-1}), in comparison to the same vibration bands (1118 and 1031 cm^{-1}) for CTS–HNT; Fig. 5F.

3.2. Swelling and degradation

Fig. 6A and B show the swelling behavior of the sponges. p-CTS displayed the highest water absorption, reaching a maximum swelling of 122% after 1 h of immersion in PBS. CTS–AgNPs sponges presented a smaller swelling capacity in comparison to p-CTS, where AgNPs concentration was inversely correlated to the water adsorption capacity of the sponges (Fig. 6A). CTS–HNT exhibited a smaller water absorption capacity (≈15% decrease in comparison to p-CTS), Fig. 6A and B, and upon incorporation of AgNPs, swelling capacity of the CTS–HNTs–AgNPs sponges further decreased as AgNPs concentration increased.

Fig. 6C and D, present the degradation of the sponges immersed in lysozyme-PBS solution for up to 21 days of immersion. p-CTS exhibited the highest degradation rate, at 4 days of immersion it lost 30% of its original weight, and by day 21 its weight loss was ≥50%. All CTS–AgNPs sponges exhibited a smaller degradation, in comparison to p-CTS. However, decrease in degradation was not significant in comparison to p-CTS, but for 10-CTS–AgNP, which at all immersion times showed a significantly smaller degradation than p-CTS. At 21 days of immersion, 10-CTS–AgNP weight loss was 12%, while weight loss for p-CTS, 01-CTS–AgNP, 02-CTS–AgNP and 05-CTS–AgNP was ≥42%. Upon HNTs incorporation into the CTS matrix, degradation rate of CTS–HNTs–AgNPs sponges significantly decreased in comparison to their corresponding sponges with no HNTs. At incubation day 7, p-CTS weight loss was 38%,

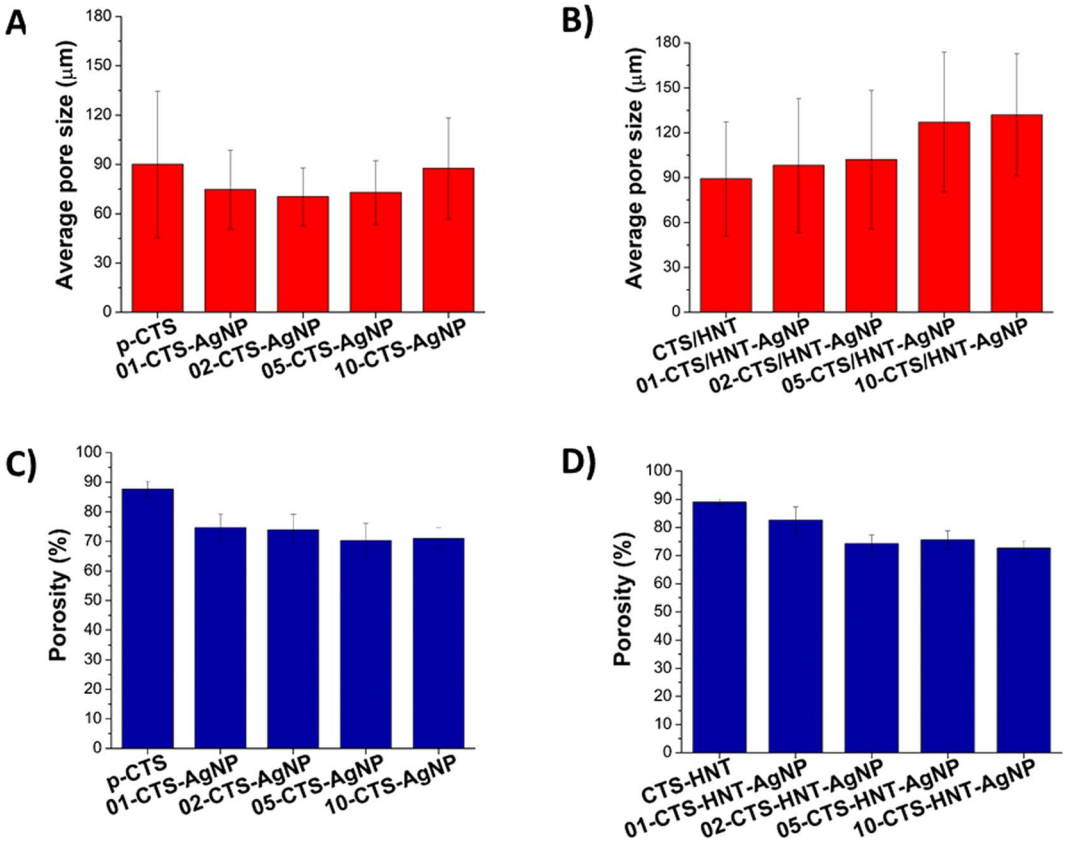

Fig. 4 (A and B) Pore size distribution and (C and D) porosity percentage of the CTS/AgNPs and CTS/HNT/AgNPs sponges.

while CTS–HNT weight loss was 25%. Decrease in degradation rate of the sponges upon HNTs incorporation was even larger when comparing the sponges containing AgNPs. At 21 days of incubation, weight loss for 01-CTS–HNT–AgNP, 02-CTS–HNT–AgNP, 05-CTS–HNT–AgNP and 10-CTS–HNT–AgNP was 25, 12, 10 and 8%, respectively, showing a significantly smaller degradation than that of their corresponding CTS–AgNPs sponges, which overall weight loss was ≥42%, except for 10-CTS–AgNP that exhibited a weight loss of 14%. Nevertheless, weight loss of 10-CTS–AgNP at 21 days of incubation (14%) was also significantly higher than that of 10-CTS–HNT–AgNP (8%) at the same incubation time.

3.3. Silver release

Cumulative silver release over time from the sponges immersed in PBS at 37 °C is shown in Fig. 6E and F. Silver release was dependent on the AgNPs concentration in the sponges, and it increased as AgNPs concentration increased. Nevertheless, the total amount and rate of silver release from CTS–HNTs–AgNPs sponges was significantly higher than their corresponding CTS–AgNPs sponges. For the two lower concentrations of AgNPs studied (either 01-CTS–AgNP and 01-CTS–HNT–AgNP or 02-CTS–AgNP and 02-CTS–HNT–AgNP), additional release of silver was no longer observed after 4 days of immersion. For 05-CTS–AgNP and 10-CTS–AgNP, and 05-CTS–HNT–AgNP and 10-CTS–HNT–AgNP an additional silver release of ≈100 and 200 ppb, respectively, occurred from immersion day 4 to immersion day 7. At 7 days of immersion, cumulative silver release was 18, 52, 215 and 320 ppb for 01-CTS–AgNP, 02-CTS–AgNP, 05-CTS–AgNP and 10-CTS–AgNP, respectively, while it was 20, 105, 400 and 522 ppb for 01-CTS–HNT–AgNP, 02-CTS–HNT–AgNP, 05-CTS–HNT–AgNP and 10-CTS–HNT–AgNP, respectively.

Table 2 Silver content in the sponges

Sponge (CTS–AgNPs)	Silver content (wt%)	Sponge (CTS–HNTs–AgNPs)	Silver content (wt%)
p-CTS	—	CTS–HNT	—
01-CTS–AgNP	0.056	01-CTS–HNT–AgNP	0.054
02-CTS–AgNP	0.081	02-CTS–HNT–AgNP	0.070
05-CTS–AgNP	0.211	05-CTS–HNT–AgNP	0.084
10-CTS–AgNP	0.651	10-CTS–HNT–AgNP	0.100

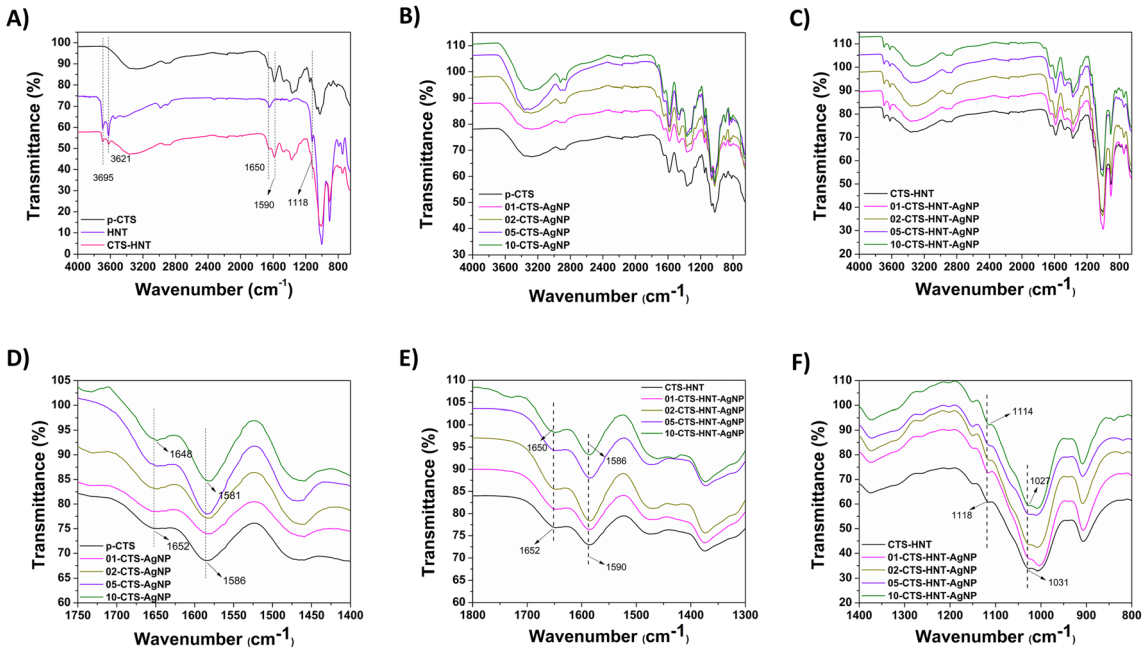

Fig. 5 FTIR spectra of (A) as received HNTs and p-CTS and CTS–HNT sponges, (B) p-CTS and CTS/AgNPs sponges, (C) CTS–HNT and CTS/HNT/AgNPs sponges. Magnification of the FTIR spectra exhibiting the (D) upshifting of the main cts bands occurring in the (D) CTS/AgNPs and (E) CTS/HNTs/AgNPs sponges. (F) Magnification of the FTIR spectra exhibiting the downshifting of the main hnts bands occurring in the CTS/HNTs/AgNPs sponges.

3.4. Mechanical properties

Table 3 shows the compressive stress of the fully hydrated sponges at 80% strain. p-CTS has the lowest compressive stress in comparison to all sponges studied. Compressive stress of CTS–AgNPs sponges increased with AgNPs concentration. For 10-CTS–AgNP compressive stress was 0.0572 MPa, which was almost 4-fold higher than that of p-CTS (0.0146 MPa). Incorporation of HNTs into the CTS matrix significantly enhanced the compressive stress of the sponges, where CTS–HNT compressive stress (0.0794 MPa) was 5.5 times higher than that of p-CTS (0.0146 MPa). AgNPs incorporation into the CTS–HNTs matrix, further increased the compressive stress of the sponges in a AgNPs concentration depending on manner. In general, CTS–HNTs–AgNPs sponges exhibited a ≈2–3 times larger compressive stress than that of their corresponding CTS–AgNPs sponges.

3.5. Antibacterial evaluation

3.5.1. Planktonic growth inhibition. Antibacterial activity of the sponges was tested against four strains of clinically-relevant pathogenic bacteria commonly found in infected wounds, Gram-negative *E. coli* and *P. aeruginosa* and Gram-positive *S. aureus* and *S. epidermidis*. Percentage of planktonic bacterial growth at 24 h of incubation in presence of the sponges is shown in Fig. 7. From Fig. 7A and B, it can be observed that p-CTS significantly inhibited the planktonic growth of Gram-negative bacteria *E. coli* and *P. aeruginosa* in comparison to Ctrl− (normal planktonic bacterial growth in presence of no sponges). CTS–HNT sponges also inhibited *E. coli* and *P. aeruginosa* planktonic growth in comparison to Ctrl−; however, this decrease was not significant. For AgNPs-containing sponges, the trend exhibited that the antibacterial activity of the sponges against *E. coli* and *P. aeruginosa* increased as AgNPs concentration increased (Fig. 7A and B); nevertheless, *P. aeruginosa* seemed to be more susceptible to AgNPs than *E. coli*. Against *E. coli* (Fig. 7A), all AgNPs-containing sponges significantly decreased the planktonic bacterial growth in comparison to Ctrl−. However, no significant difference was observed between the antibacterial activity of the sponges containing AgNPs and that of their corresponding non-AgNPs base sponge (either p-CTS or CTS–HNT), except for the largest AgNPs concentration studied, 10-CTS–AgNP and 10-CTS–HNT–AgNP, which exhibited a significantly higher antibacterial activity than all the other sponges studied. 10-CTS–HNT–AgNP exerted a significantly higher inhibition of bacterial planktonic growth than 10-CTS–AgNP. Against *P. aeruginosa* (Fig. 7B), antibacterial activity of the sponges significantly improved, showing a larger inhibition of planktonic bacterial growth as AgNPs concentration increased; 05-CTS–AgNP, 10-CTS–AgNP and 10-CTS–HNT–AgNP completely inhibited *P. aeruginosa* planktonic growth.

For Gram-positive bacteria *S. aureus* (Fig. 7C), p-CTS and CTS–HNT significantly decreased (by ≈70%) *S. aureus* planktonic growth, in comparison to Ctrl−. The antibacterial activity further increased with AgNPs concentration in the sponges; almost complete inhibition of *S. aureus* planktonic growth was observed from 02-CTS–AgNP and 05-CTS–HNT–AgNP. In the case of Gram-positive bacteria *S. epidermidis*, planktonic bacterial growth was not inhibited by neither p-CTS nor CTS–

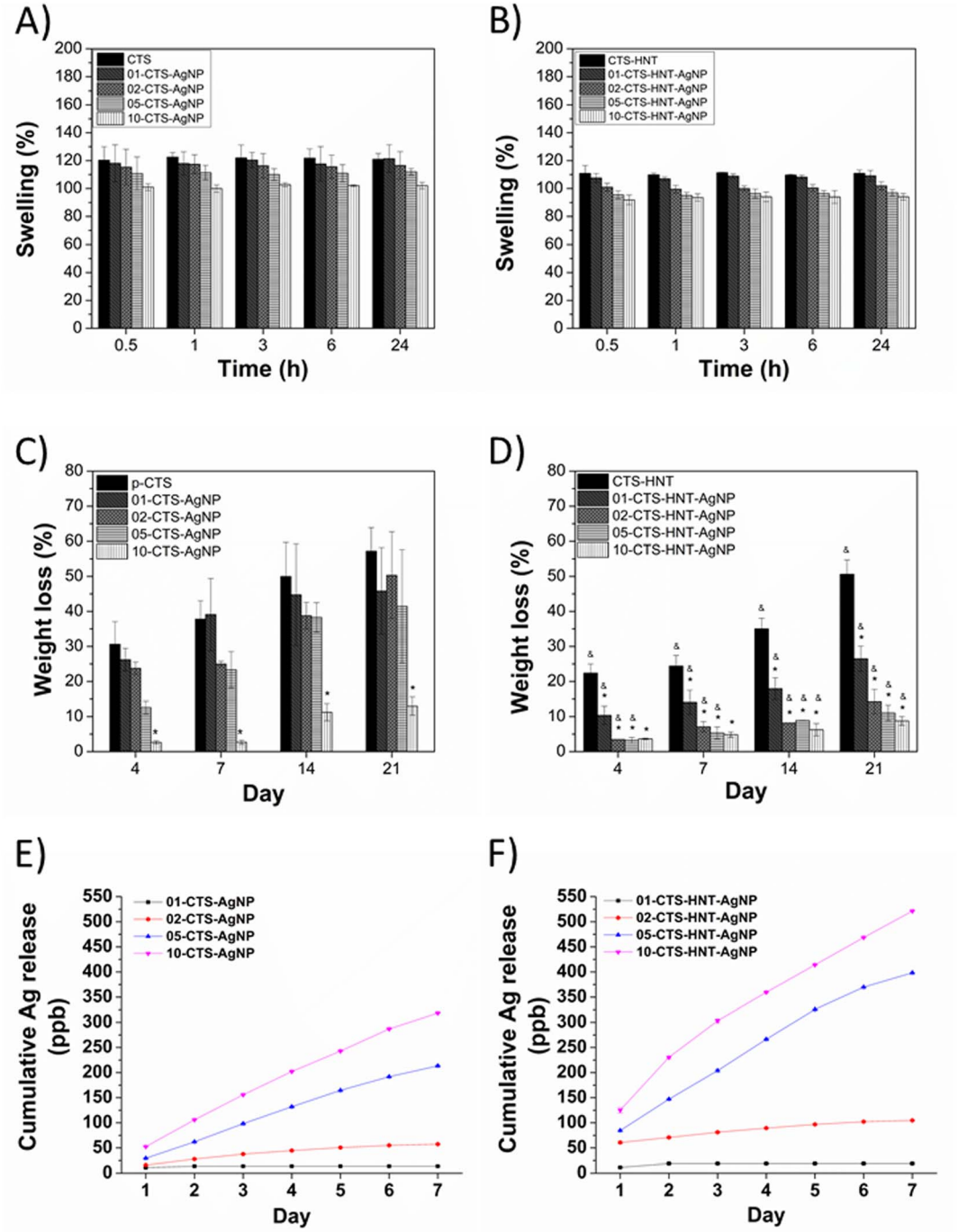

Fig. 6 (A and B) Water absorption capacity (swelling percentage) of the sponges, (C and D) degradation rate of the sponges incubated in PBS-lysozyme solution, and (E and F) cumulative silver release from the sponges immersed in PBS.

Table 3 Mechanical properties of the sponges in their fully hydrated state

Sponge (CTS–AgNPs)	Compressive stress at 80% strain (MPa)	Sponge (CTS–HNTs–AgNPs)	Compressive stress at 80% strain (MPa)
CTS	0.0146 ± 0.0031	CTS–HNT	0.0794 ± 0.0026
01-CTS–AgNP	0.0275 ± 0.0016	01-CTS–HNT–AgNP	0.0801 ± 0.0075
02-CTS–AgNP	0.0378 ± 0.0023	02-CTS–HNT–AgNP	0.0937 ± 0.0045
05-CTS–AgNP	0.0459 ± 0.0083	05-CTS–HNT–AgNP	0.1211 ± 0.0018
10-CTS–AgNP	0.0572 ± 0.0009	10-CTS–HNT–AgNP	0.1739 ± 0.0235

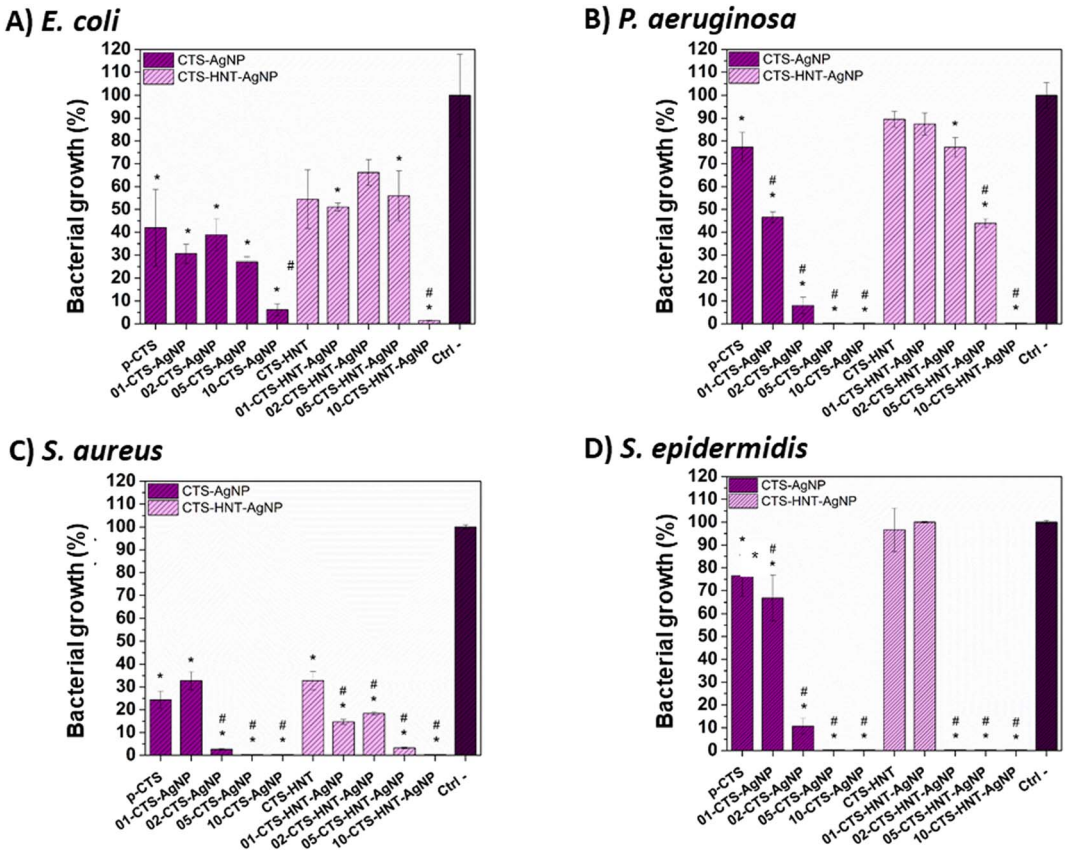

Fig. 7 Inhibition of (A) *E. coli*, (B) *P. aeruginosa*, (C) *S. aureus* and (D) *S. epidermidis* planktonic growth, as percentage of viable bacteria at 24 h of incubation in presence of the sponges; 100% viable bacteria corresponds to Ctrl− (no antibacterial activity; *i.e.* standard bacteria culture conditions). *, $p < 0.05$ *vs.* Ctrl−; #, $p < 0.05$ *vs.* base sponge with no agnps, either p-CTS or CTS–HNT correspondingly.

HNT; Fig. 7D. However, *S. epidermidis* planktonic growth was drastically inhibited from 02-CTS–AgNP and 02-CTS–HNT–AgNP, with complete inhibition exerted from 05-CTS–AgNP and 02-CTS–HNT–AgNP.

3.5.2. Adherent growth inhibition. Since bacterial adhesion is the first step into biofilm formation or colonial growth of adherent bacteria, which is the more common form of bacterial growth in nature, and it has been found in the tissues of patients with different infections and chronic wounds,[78] the potential of the sponges to prevent the adhesion and growth of adherent bacteria was tested. Fig. 8 shows percentage of viable bacteria adhered to the sponges after 24 h of incubation in presence of bacteria inoculum. In the case of *E. coli* (Fig. 8A), p-CTS, 01-CTS–AgNP, 02-CTS–AgNP and 05-CTS–AgNP showed a similar adhesion of viable bacteria as that observed for Ctrl− (viable bacteria adhered to the standard culture well plate in presence of no sponges). A significant decrease in percentage of viable bacteria adhered, in comparison to Ctrl−, was only observed for 10-CTS–AgNP. For HNTs-containing sponges, 05-CTS–HNT–AgNP and 10-CTS–HNT–AgNP significantly decreased percentage of viable bacteria adhered, in comparison to Ctrl−, in a trend where viable bacteria adhered decreased as AgNPs concentration increased.

Against *P. aeruginosa*, p-CTS significantly reduced viable bacteria adhesion in comparison to Ctrl−; Fig. 8B. All CTS–AgNPs sponges, but 01-CTS–AgNPs, exhibited ≈50% reduction of bacteria adhered in comparison to Ctrl−, and significantly reduced percentage of viable bacteria adhered to the sponges in comparison to p-CTS; however, none of the AgNPs concentrations studied completely inhibited adhesion of viable bacteria. Presence of HNTs into the sponges slightly decreased their antibacterial capacity, in comparison with the corresponding sponges with no HNTs. 05-CTS–HNT–AgNP and 10-CTS–HNT–AgNP significantly increased inhibition of *P. aeruginosa* adhesion, in comparison to Ctrl− and CTS–HNT. None of the CTS–HNTs–AgNPs sponges completely inhibited *P. aeruginosa* adhesion.

For *S. aureus* (Fig. 8C), neither p-CTS, 01-CTS–AgNP, CTS–HNT nor 01-CTS–HNT showed any decrease on bacterial adhesion, showing a similar bacterial adhesion to that of Ctrl−. 02-CTS–AgNP, 05-CTS–AgNP and 10-CTS–AgNP completely inhibited *S. aureus* adhesion. For HNTs-containing sponges, adhesion of viable bacteria decreased by 60% on 02-CTS–HNT–AgNP in comparison to Ctrl−, and further decrements were observed for the CTS–HNTs–AgNPs sponges with larger AgNPs concentration, reaching total inhibition of viable bacterial adhesion for 10-CTS–HNT–AgNP.

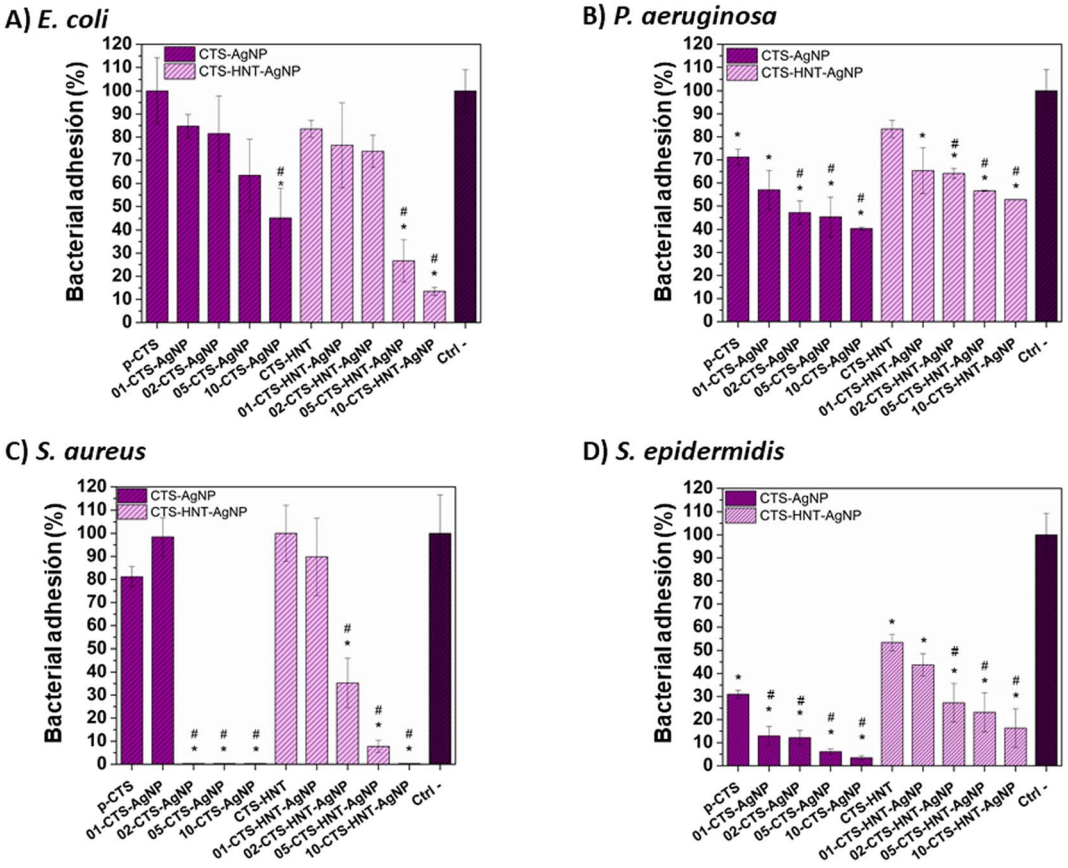

Fig. 8 Inhibition of (A) *E. coli*, (B) *P. aeruginosa*, (C) *S. aureus* and (D) *S. epidermidis* biofilm formation as percentage of viable bacteria adhered to the sponges at 24 h of incubation in presence of the sponges; 100% viable bacteria correspond to bacteria adhered to Ctrl− (no antibacterial activity; *i.e.* standard culture plate surface with no sponges). *, $p < 0.05$ *vs.* Ctrl−; #, $p < 0.05$ *vs.* base sponge with no agnps, either p-CTS or CTS–HNT, correspondingly.

Against *S. epidermidis* (Fig. 8D), all the sponges studied, with or without AgNPs, evidenced a significant inhibition of viable bacterial adhesion in comparison to Ctrl−. HNTs-containing sponges exhibited a smaller antibacterial effect in comparison to their corresponding sponges with no HNTs. Improvement of the inhibition of bacterial adhesion on the sponges was observed as AgNPs concentration increased, for CTS and CTS–HNTs base sponges, until 96% and 84% decrease in *S. epidermidis* bacterial adhesion was reached on 10-CTS–AgNP and 10-CTS–HNT–AgNP, respectively.

3.5.3. Inhibition halos. The antibacterial activity of the sponges was also studied by the disk-diffusion test; p-CTS and CTS–HNT sponges impregnated with chlorhexidine gluconate were used as antibacterial Ctrl+. All sponges exhibited antibacterial activity against all tested bacteria; however, zone of inhibition was dependent on AgNPs concentration and HNT content; Fig. S2 and Table S1.† Sponges with HNT and the higher AgNPs concentrations showed the larger inhibition zones and were particularly effective against *P. aeruginosa* and *S. epidermidis*; 05-CTS–HNT–AgNP and 10-CTS–HNT–AgNP exhibited inhibition halos significantly larger than that of CTS–HNT. In the case of the sponges with no HNTs, all sponges, including p-CTS, displayed similar antibacterial effects where zones of inhibition were limited to the diameter of the sponges only.

3.6. Cytocompatibility evaluation using fibroblasts

Fluorescence micrographs (calcein-AM/ethidium homodimer assay) acquired at 8 days of human fibroblasts culture on the sponges are shown in Fig. 9A and fluorescence semiquantitative analysis is shown in Fig. 9B. Cell viability on p-CTS and CTS–HNT was ≥95%, and cells were distributed overall the 3D structure of the sponges; however, a larger number of cells with the characteristic spindle-like morphology of well adhered fibroblast were observed on p-CTS, in comparison to CTS–HNT. AgNPs presence in the sponges decreased cell viability and the number of cells on the sponges in a AgNPs concentration-dependent manner. 10-CTS–AgNP and 10-CTS–HNT–AgNP exhibited a significantly smaller cell viability percentage (58% and 78%, respectively), in comparison to p-CTS and CTS–HNT, respectively. Presence of HNTs in the sponges had a positive effect on cell viability and expected cell morphology for fibroblasts. A larger number of viable cells, distributed over the 3D structure of the sponge, was observed on CTS–HNTs–AgNPs sponges in comparison with corresponding CTS–AgNPs sponges. Nevertheless, differences in cell viability percentage when comparing 01-CTS–HNT–AgNP *vs.* 01-CTS–AgNP, 02-CTS–HNT–AgNP *vs.* 02-CTS–AgNP, 05-CTS–HNT–AgNP *vs.* 05-CTS–AgNP and 10-CTS–HNT–AgNP *vs.* 10-CTS–AgNP were not

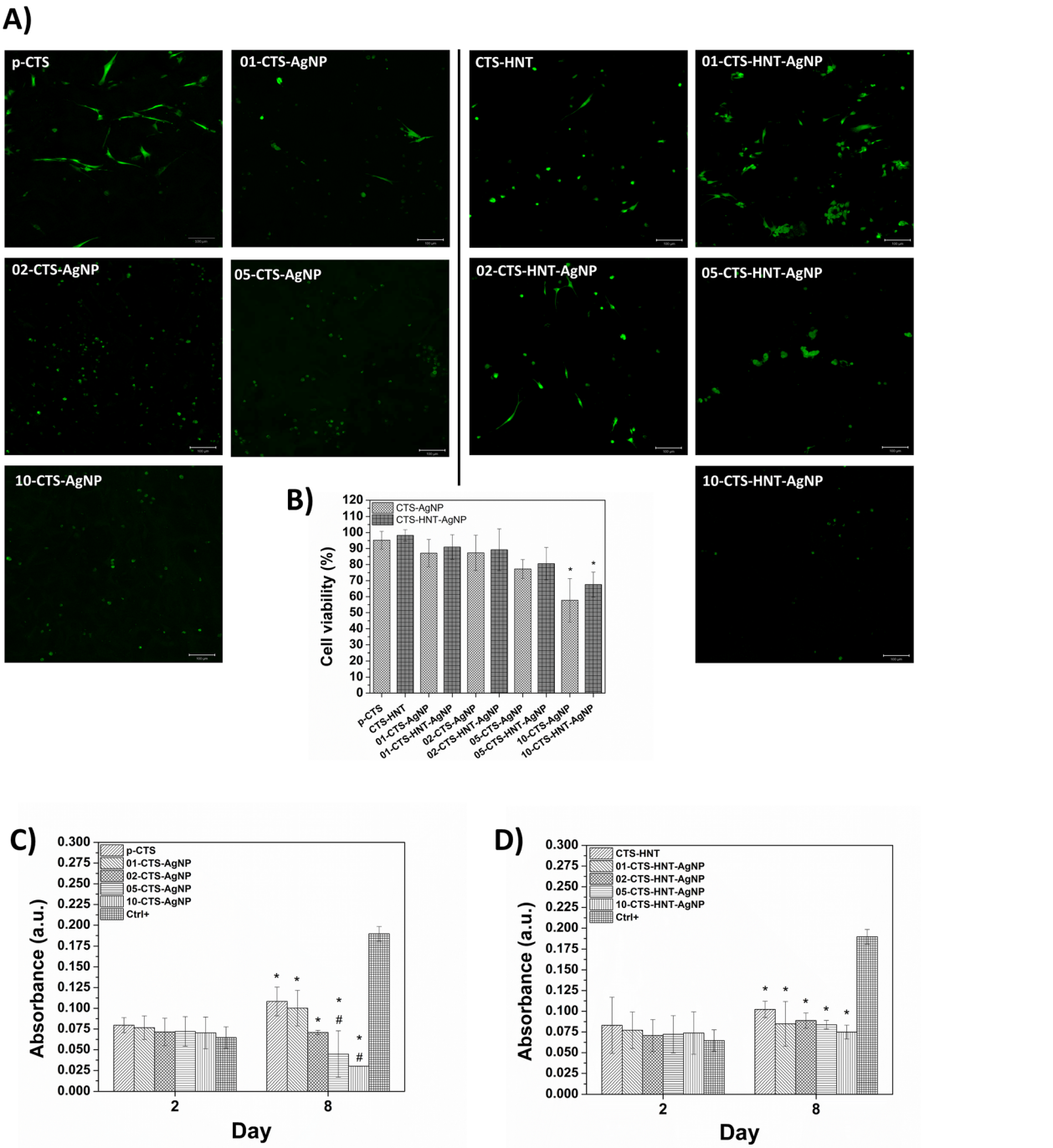

Fig. 9 (A) Fluorescent images of HF cells on CTS/AgNP and CTS/HNT–AgNP sponges at 8 days of culture; viable (green fluorescence) and non-viable (red fluorescence) cells are observed. (B) Percentage of viable cells on the sponges according to fluorescent images. absorbance measurements from MTT assay on HF cells cultured for 2 and 4 days on (C) CTS/AgNP and (D) CTS/HNT/AgNP sponges.

statistically significant; Fig. 9B. Cells exhibited a more extended spindle-like morphology on CTS–HNTs–AgNPs sponges than on corresponding CTS–AgNPs sponges. Cells with an extended morphology can be observed for up to 05-CTS–HNT–AgNP, while cells on CTS–AgNPs sponges did not present an extended morphology from 02-CTS–AgNP.

To confirm the semi-quantitative observations from calcein-AM/ethidium homodimer assay, MTT tests were performed at 2 and 8 days of cell culture on independent sponge samples, Fig. 9C and D. At 2 days of cell culture, MTT assay absorbance reads were similar between the Ctrl+ and all the sponges tested, independently of AgNPs and/or HNTs content. A slight trend for decreasing absorbance was observed with increasing AgNPs concentration in the sponges, for both CTS–HNTs–AgNPs and CTS–AgNPs sponges; however, differences were not statistically significant. At 8 days of cell culture absorbance reads from p-

CTS and all CTS–AgNPs sponges were significantly smaller than Ctrl+, with absorbance decreasing as AgNP concentration increased; absorbance reads from 05-CTS–AgNP and 10-CTS–AgNP were also significantly smaller than p-CTS. Absorbance reads from p-CTS, 01-CTS–AgNP and 02-CTS–AgNP at 8 days of cell culture were higher than those concerning measurements at 2 days of cells culture on the same sponges, indicating that the number of viable cells on the sponges increased with culture time. At 8 days of cell culture on HNTs-containing sponges, absorbance reads were also significantly smaller than Ctrl+; nevertheless, an increment in absorbance was observed when comparing between the same sponges at 2 days of cell culture. In addition, absorbance reads were higher for 02-CTS–HNT–AgNP, 05-CTS–HNT–AgNP and 10-CTS–HNT–AgNP in comparison to their corresponding sponges with no HNTs.

Finally, immunofluorescence assays against α-SMA were performed at 8 days of cell culture on the sponges that showed the higher cytocompatibility (cell viability) according to the MTT assay, that is, p-CTS, CTS–HNT, 01-CTS–AgNP, 01-CTS–HNT–AgNP, 02-CTS–AgNP and 02-CTS–HNT–AgNP. Fig. 10 shows representative confocal images of this immunoassay. It can be noted that AgNPs presence in the sponges increase α-SMA expression. On p-CTS, ≈20% of cells exhibited positive α-SMA expression, while 35% of cells were positive for α-SMA on 01-CTS–AgNP and 02-CTS–AgNP. For the sponges containing HNTs, percentage of cells positive to α-SMA did not change with AgNPs presence in the sponges; α-SMA-positive cells percentage was similar (≈33%) for CTS–HNT, 01-CTS–HNT–AgNP and 02-CTS–HNT–AgNP, and also to p-CTS.

4. Discussion

Here CTS-based composite sponges containing AgNPs were prepared *via in situ* reduction process using CTS as reduction and stabilizing agent. To increase the mechanical properties of the sponges and hoping to improve the distribution and avoiding the agglomeration of the AgNPs in the nanocomposites, a constant HNTs concentration was added, and therefore, two groups of sponges were obtained: (i) CTS–AgNPs and (ii) CTS–HNTs–AgNPs nanocomposites. Four different concentrations of silver precursor were used, finally obtaining four different AgNPs-containing sponges per each group, in addition to the non-AgNPs control sponges for each group, p-CTS and CTS–HNT. Synthesized AgNPs had different size

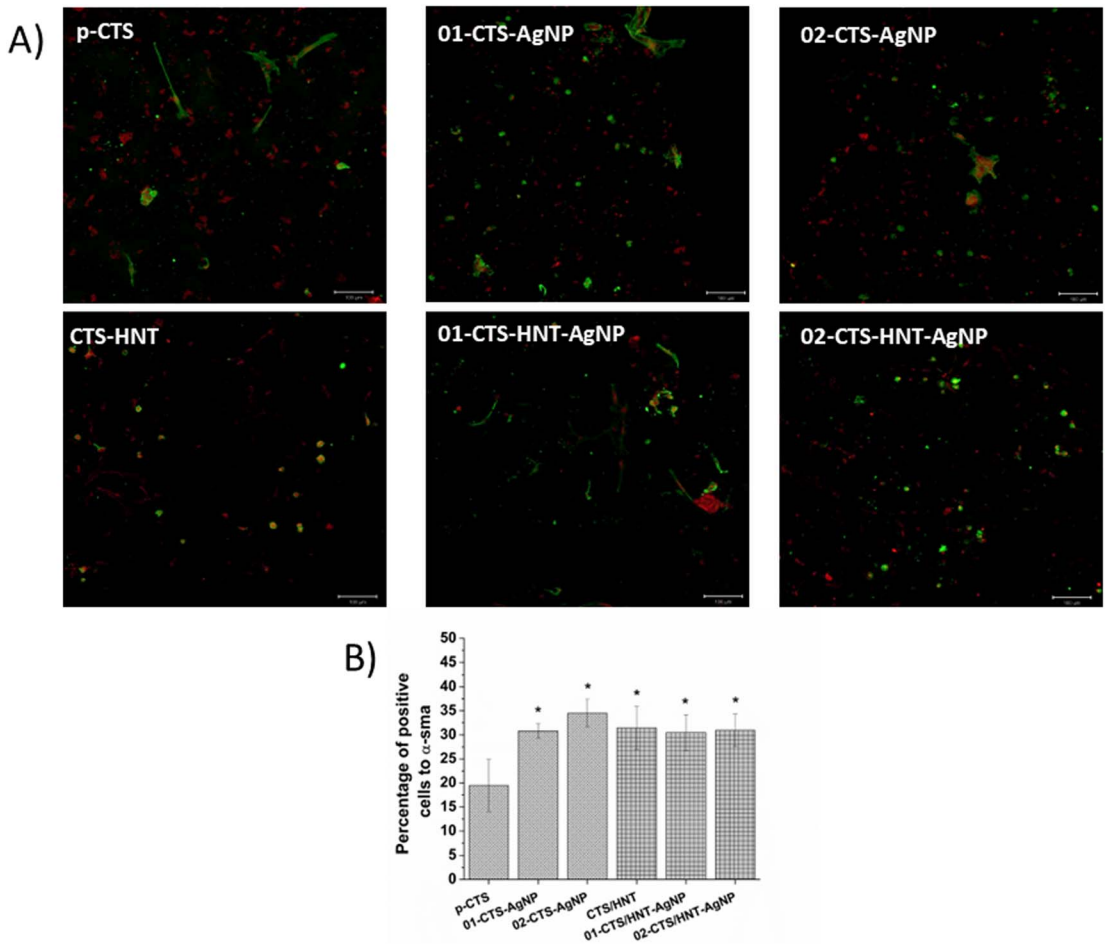

Fig. 10 (A) Immunofluorescence images of α-SMA expression for HF cells cultured on the sponges during 8 days. Red signal shows the cell nuclei and green signal the positive expression of α-SMA. (B) Quantitative analysis of percentage of cells exhibiting positive α-SMA expression.

distributions depending on the silver precursor concentration, as silver precursor concentration increased smaller nanoparticles were obtained. This effect can be explained by a greater quantity of silver precursor presenting more nucleation sites for AgNPs synthesis, and thus, the highest availability of nucleation sites resulting in a more controlled growth of AgNPs with smaller diameter as silver precursor concentration increase.[79,80] With addition of HNTs, there was a marked reduction in the average size of the synthesized AgNPs, resulting in 50% smaller AgNPs with narrower size distribution for CTS–HNTs–AgNPs than for CTS–AgNPs nanocomposites. In addition to generating a larger number of nucleation sites with increasing silver precursor concentration, the addition of HNTs resulted in a more viscous CTS–HNT solution than CTS-only solution, which might prevent the agglomeration, and the subsequent larger growth, of the synthesized AgNPs.[79,80] FTIR spectroscopy corroborated that AgNPs had a dual chemical interaction in the CTS–HNTs–AgNPs sponges, that is, not only CTS interacts with the AgNPs through its $-NH_3$ groups, mainly, but also HNTs interact with the AgNPs acting as further anchoring sites for the nanoparticles. This effect has been previously demonstrated by studies showing the positive effect of HNTs acting as immobilization sites for different metallic nanoparticles in general, and for AgNPs in particular, improving AgNPs dispersion and controlling their average size during synthesis.[57,73,81,82]

The addition of nano-fillers in CTS matrices is a method to increase its mechanical properties, and consequently a method to improve their degradation rate and handling at physiological conditions, and overall, their capacity to support cell culture conditions.[22,24,83,84] CTS–HNT sponges showed a more homogeneous pore structure and fewer collapsed areas in the pore walls in comparison with p-CTS, which can be attributed to the strong interactions between CTS and HNTs. In acidic medium strong electrostatic interactions between the positively charged amino groups of CTS and the negatively charged outer surface of HNTs occur,[35,36] improving the mechanical properties of the sponges by increasing their rigidity, and significantly decreasing their degradation rate.

The sudden, total, and uncontrolled release of the silver content of silver-based antibacterial-intended wound dressings is undesirable for several reasons, but mainly because a large abrupt release of silver into tissues can be significantly cytotoxic (depending on the concentration released), and because the antibacterial activity of the dressings would be rapidly lost upon total sudden release of their silver content.[85,86] Silver released into wounds can be rapidly deactivated, losing its antibacterial properties due to their complexation with proteins or chloride ions present on the surface of wounds.[52] For the present sponges, a larger silver release was observed from the sponges containing HNTs, even when the total silver concentration in CTS–HNTs–AgNPs sponges was smaller than that in their corresponding CTS–AgNPs sponges synthesized with the same concentration of silver precursor. Thus, the higher silver release observed from CTS–HNTs–AgNPs sponges was not related to the silver concentration of the sponges, but it could had been more related to the size of the AgNPs in each different sponge group (with HNTs or without HNTs).[87,88] As shown by TEM results, the addition of HNTs to the nanocomposites resulted in smaller AgNPs. Since surface contact area increases as AgNPs size decreases, the reactivity and release of smaller AgNPs upon the immersion of the sponges in aqueous media might increase due to a larger total surface contact area.[87,88] Resulting in CTS–HNTs–AgNPs sponges releasing a larger amount of silver, in comparison to corresponding CTS–AgNPs sponges at the same days of immersion in aqueous medium. Nevertheless, it is important to emphasize that cytocompatibility of the sponges seemed to be more related to their silver concentration than to their silver release rate. In this respect, at 8 days of cell culture on the sponges, CTS–HNTs–AgNPs sponges, presenting a larger silver release rate, exhibited a higher cell viability (by both calcein AM/ethidium homodimer and MTT assays), in comparison to their corresponding CTS–AgNPs sponges synthesized using the same concentration of silver precursor, which presented a smaller silver release rate but a larger silver concentration. Nonetheless, total silver concentration in the sponges and silver release rates observed for 01-CTS–AgNP and 02-CTS–AgNP, and 01-CTS–HNT–AgNP, 02-CTS–HNT–AgNP, 05-CTS–HNT–AgNP, 10-CTS–HNT–AgNP did not exert a significantly cytotoxic effect on human fibroblasts (as a model of the main cell phenotype in the dermis layer of the skin) concerning p-CTS or CTS–HNT at 8 days of cell culture.

On the other hand, the improved antibacterial effects observed for CTS–AgNPs and CTS–HNTs–AgNPs sponges were correlated with higher concentrations of AgNPs, in a general trend for all the bacteria strains tested. Sponges with AgNPs showed improved antibacterial effects against all strains of bacteria tested, as compared to p-CTS or CTS–HNT. However, the significance of the antibacterial effects observed was dependent on the AgNPs concentration, the presence of HNTs in the sponges, and the specific bacteria strain tested. The results were consistent for the two antibacterial effects studied (inhibition of floating and adhered growth), indicating that CTS–AgNPs and CTS–HNTs–AgNPs sponges, inhibited bacterial planktonic growth and prevented viable bacteria adhesion on the sponges. Inhibiting the planktonic (floating) growth of bacteria is a good indication of the antibacterial properties of the nanocomposites; however, bacteria normally growth in nature and in infected sites or chronic wounds as colonial adhered bacteria, thus testing the antibacterial capacity of the nanocomposites to inhibit the adhesion of viable bacteria, as the first step into colonial adherent growth, is also important to further asses the antibacterial properties of the nanocomposite sponges.[78,89] Presence of HNTs in the sponges slightly decreased their antibacterial effect in comparison with corresponding sponges with no HNTs but synthesized with the same concentration of silver precursor. This can be correlated to the fact that the HNTs nanotubes interacted with the AgNPs, as demonstrated by the FT-IR analysis. This interaction somehow decreased the total silver concentration in the CTS–HNTs-based sponges, in comparison with corresponding CTS-based sponges, and might had hindered the direct interaction between the AgNPs and the cell wall of the tested bacteria, decreasing the AgNPs contact area, and therefore, their antibacterial activity. The less sensitive bacteria strain to the

sponges was *E. coli*. CTS–AgNPs and CTS–HNTs–AgNPS significantly inhibited the planktonic growth and adhesion of Gram-positive *S. aureus* and *S. Epidermidis* from 02-CTS–AgNP and 02-CTS–HNT–AgNP and sponges with higher silver concentrations. Against Gram-negative *P. aeruginosa* similar results were observed and significant antibacterial effects were exerted from 02-CTSAgNP and 05-CTS–HNT–AgNP and higher silver concentrations.

5. Conclusions

Overall results suggest that developed CTS–AgNPs and CTS–HNTs–AgNPs sponges: (a) present favorable degradation and mechanical properties as scaffolds for potential wound dressing applications; (b) are expected to retain their antibacterial action over time upon a possible application as scaffolds for potential wound dressing applications, since releasing silver in a controlled manner upon immersion in aqueous an enzymatic media at 37 °C; (c) do not represent potential cytotoxic materials considering that the silver release for all the sponges was in the order of parts per billion per day, and that the all the sponges, except for the higher silver concentrations studied 10-CTS–AgNP and 10-CTS–HNT–AgNP, properly supported human fibroblasts culture, and (d) represent antibacterial materials capable of inhibiting planktonic and colonial adherent bacteria growth, against different Gram-negative and Gram-Positive bacteria strains. Constituting prospective scaffold materials for potential wound dressing applications with simultaneous adequate cytocompatibility and antibacterial properties, mainly 02-CTS–AgNP and 05-CTS–AgNP, and 02-CTS–HNT–AgNP, 05-CTS–HNT–AgNP and 10-CTS–AgNPs.

Data availability

The authors confirm that the data supporting the findings of this study are available within the article and ESI.†

Conflicts of interest

The authors declare no conflict of interest.

Acknowledgements

This research was financially supported by CONACyT under the projects FOSIS-161687 and CONACyT-Texas/CONTEX 108 and IPN under the project SIP-20240845. A. Hernandez-Rangel acknowledges postdoctoral fellowship from CONACyT. Authors are also grateful to X. Guerrero (INR-LGII) for their technical support, R.A. Mauricio Sanchez and E. Gutierrez Arias (CINVESTAV-Queretaro) for assistance with FTIR and ICP-OES measurements, A.D. Hernández Pérez (INR-LGII) for TEM images, L. Tamay de Dios (INR-LGII) for confocal microscopy images and J. García-López (INR-LGII) for help with immunofluorescence assays.

References

1 E. M. Tottoli, R. Dorati, I. Genta, E. Chiesa, S. Pisani and B. Conti, *Pharmaceutics*, 2020, **12**, 735.
2 I. Negut, G. Dorcioman and V. Grumezescu, *Polymers*, 2020, **12**, 2010.
3 S. Sepahi, M. Kalaee, S. Mazinani, M. Abdouss and S. M. Hosseini, *J. Nanostruct. Chem.*, 2021, **11**, 245–258.
4 L. Suamte, A. Tirkey and P. J. Babu, *Smart Mater. Med.*, 2023, **4**, 243–256.
5 S. Murugesan and T. Scheibel, *J. Polym. Sci.*, 2021, **59**, 1610–1642.
6 S. K. L. Levengood and M. Zhang, *J. Mater. Chem. B*, 2014, **2**, 3161.
7 J. Zhao, P. Qiu, Y. Wang, Y. Wang, J. Zhou, B. Zhang, L. Zhang and D. Gou, *Int. J. Biol. Macromol.*, 2023, **244**, 125250.
8 A. Biswal, S. S. Purohit and S. K. Swain, *J. Drug Delivery Sci. Technol.*, 2023, **84**, 104549.
9 M. Rinaudo, *Prog. Polym. Sci.*, 2006, **31**, 603–632.
10 B. S. Anisha, D. Sankar, A. Mohandas, K. P. Chennazhi, S. V. Nair and R. Jayakumar, *Carbohydr. Polym.*, 2013, **92**, 1470–1476.
11 V. Ambrogi, A. Donnadio, D. Pietrella, L. Latterini, F. A. Proietti, F. Marmottini, G. Padeletti, S. Kaciulis, S. Giovagnoli and M. Ricci, *J. Mater. Chem. B*, 2014, **2**, 6054.
12 F. Croisier and C. Jérôme, *Eur. Polym. J.*, 2013, **49**, 780–792.
13 M. Ul-Islam, K. F. Alabbosh, S. Manan, S. Khan, F. Ahmad and M. W. Ullah, *Adv. Ind. Eng. Polym. Res.*, 2024, **7**, 79–99.
14 H. P. S. Abdul Khalil, C. K. Saurabh, A. S. Adnan, M. R. Nurul Fazita, M. I. Syakir, Y. Davoudpour, M. Rafatullah, C. K. Abdullah, M. K. M. Haafiz and R. Dungani, *Carbohydr. Polym.*, 2016, **150**, 216–226.
15 K.-J. Kim, W. S. Sung, S.-K. Moon, J.-S. Choi, J. G. Kim and D. G. Lee, *J. Microbiol. Biotechnol.*, 2008, **18**, 1482–1484.
16 M. Ji, J. Li, Y. Wang, F. Li, J. Man, J. Li, C. Zhang, S. Peng and S. Wang, *Carbohydr. Polym.*, 2022, **297**, 120058.
17 S. K. Soni, B. Thomas, S. B. Thomas, P. S. Tile and S. G. Sakharwade, *Mater. Today Commun.*, 2023, **37**, 107358.
18 U. Marathe, M. Padhan and J. Bijwe, *Compos. Sci. Technol.*, 2021, **210**, 108813.
19 M. Cobos, B. González, M. J. Fernández and M. D. Fernández, *J. Appl. Polym. Sci.*, 2017, **134**, 1–14.
20 Z. Sun, K. Hu, T. Wang, X. Chen, N. Meng, X. Peng, L. Ma, D. Tian, S. Xiong, C. Zhou and Y. Yang, *Int. J. Biol. Macromol.*, 2024, **266**, 131277.
21 Y. Wang, S. Liu and W. Yu, *Macromol. Biosci.*, 2021, **21**, 2000432.
22 S. Kouser, A. Prabhu, K. Prashantha, G. K. Nagaraja, J. N. D'souza, K. Meghana Navada, A. Qurashi and D. J. Manasa, *Colloids Surf., A*, 2022, **634**, 127941.
23 B. Huang, M. Liu, Z. Long, Y. Shen and C. Zhou, *Mater. Sci. Eng., C*, 2017, **70**, 303–310.
24 D. Huang, Z. Zhang, Y. Zheng, Q. Quan, W. Wang and A. Wang, *Food Hydrocolloids*, 2020, **101**, 105471.

25 S. Wang, F. Hu, J. Li, S. Zhang, M. Shen, M. Huang and X. Shi, *Nanomed. Nanotechnol. Biol. Med.*, 2018, **14**, 2505–2520.
26 W. Wei, M. Wang, Z. Liu, W. Zheng, P.-L. Tremblay and T. Zhang, *Carbohydr. Polym.*, 2024, **324**, 121507.
27 V. de, A. M. Gonzaga, A. L. Poli, J. S. Gabriel, D. Y. Tezuka, T. A. Valdes, A. Leitão, C. F. Rodero, T. M. Bauab, M. Chorilli and C. C. Schmitt, *J. Biomed. Mater. Res., Part B*, 2020, **108**, 1388–1397.
28 S. Same, S. A. Nakhjavani, G. Samee, G. Navidi, Y. Jahanbani and S. Davaran, *Ceram. Int.*, 2022, **48**, 31065–31079.
29 K. Fakhruddin, R. Hassan, M. U. A. Khan, S. N. Allisha, S. I. A. Razak, M. H. Zreaqat, H. F. M. Latip, M. N. Jamaludin and A. Hassan, *Arabian J. Chem.*, 2021, **14**, 103294.
30 K. Madhusudana Rao, A. Kumar and S. S. Han, *Mater. Lett.*, 2018, **213**, 231–235.
31 E. Gkouma, E. Gianni, K. Avgoustakis and D. Papoulis, *Appl. Clay Sci.*, 2021, **214**, 106291.
32 G. Sandri, C. Aguzzi, S. Rossi, M. C. Bonferoni, G. Bruni, C. Boselli, A. I. Cornaglia, F. Riva, C. Viseras, C. Caramella and F. Ferrari, *Acta Biomater.*, 2017, **57**, 216–224.
33 M. Massaro, R. Noto and S. Riela, *Molecules*, 2020, **25**, 4863.
34 S. Same, S. A. Nakhjavani, G. Samee, G. Navidi, Y. jahanbani and S. Davaran, *Ceram. Int.*, 2022, **48**, 31065–31079.
35 L. Lisuzzo, G. Cavallaro, S. Milioto and G. Lazzara, *Polymers*, 2020, **12**, 1766.
36 B. Čalija, J. Milić, N. Milašinović, A. Daković, K. Trifković, J. Stojanović and D. Krajišnik, *J. Appl. Polym. Sci.*, 2020, **137**, 48406.
37 M. Liu, C. Wu, Y. Jiao, S. Xiong and C. Zhou, *J. Mater. Chem. B*, 2013, **1**, 2078.
38 M. Liu, Y. Shen, P. Ao, L. Dai, Z. Liu and C. Zhou, *RSC Adv.*, 2014, **4**, 23540–23553.
39 G. Sandri, A. Faccendini, M. Longo, M. Ruggeri, S. Rossi, M. C. Bonferoni, D. Miele, A. Prina-Mello, C. Aguzzi, C. Viseras and F. Ferrari, *Pharmaceutics*, 2020, **12**, 179.
40 S. Kouser, A. Prabhu, S. Sheik, K. Prashantha, G. K. Nagaraja, J. Neetha D'souza, K. M. Navada and D. J. Manasa, *Appl. Surf. Sci. Adv.*, 2021, **6**, 100158.
41 K. Wang, S. Pan, Z. Qi, P. Xia, H. Xu, W. Kong, H. Li, P. Xue, X. Yang and C. Fu, *Adv. Mater. Sci. Eng.*, 2020, **2020**, 1–13.
42 C. Mendes, A. Thirupathi, M. E. A. B. Corrêa, Y. Gu and P. C. L. Silveira, *Int. J. Mol. Sci.*, 2022, **23**, 15376.
43 A. Uberoi, A. McCready-Vangi and E. A. Grice, *Nat. Rev. Microbiol.*, 2024, **22**, 507–521.
44 C. K. Sen, *Adv. Wound Care*, 2019, **8**, 39–48.
45 L. G. Ribeiro, G. S. C. Roque, R. Conrado and A. O. De Souza, *Antibiotics*, 2023, **12**, 91.
46 B. Szerencsés, N. Igaz, Á. Tóbiás, Z. Prucsi, A. Rónavári, P. Bélteky, D. Madarász, C. Papp, I. Makra, C. Vágvölgyi, Z. Kónya, I. Pfeiffer and M. Kiricsi, *BMC Microbiol.*, 2020, **20**, 176.
47 S. Mansoor, I. Zahoor, T. R. Baba, S. A. Padder, Z. A. Bhat, A. M. Koul and L. Jiang, *Frontal Nanotechnol.*, 2021, **3**, 1–12.
48 Y. Jian, X. Chen, T. Ahmed, Q. Shang, S. Zhang, Z. Ma and Y. Yin, *J. Adv. Res.*, 2022, **38**, 1–12.
49 T. Bruna, F. Maldonado-Bravo, P. Jara and N. Caro, *Int. J. Mol. Sci.*, 2021, **22**, 7202.
50 Y. N. Slavin, K. Ivanova, J. Hoyo, I. Perelshtein, G. Owen, A. Haegert, Y.-Y. Lin, S. LeBihan, A. Gedanken, U. O. Häfeli, T. Tzanov and H. Bach, *ACS Appl. Mater. Interfaces*, 2021, **13**, 22098–22109.
51 E. Luna-Hernández, M. E. Cruz-Soto, F. Padilla-Vaca, R. A. Mauricio-Sánchez, D. Ramirez-Wong, R. Muñoz, L. Granados-López, L. R. Ovalle-Flores, J. L. Menchaca-Arredondo, A. Hernández-Rangel, E. Prokhorov, J. L. García-Rivas, B. L. España-Sánchez and G. Luna-Bárcenas, *Int. J. Biol. Macromol.*, 2017, **105**, 1241–1249.
52 A. Hernández-Rangel, P. Silva-Bermudez, B. L. España-Sánchez, E. Luna-Hernández, A. Almaguer-Flores, C. Ibarra, V. I. Garcia-Perez, C. Velasquillo and G. Luna-Barcenas, *Mater. Sci. Eng., C*, 2019, **94**, 750–765.
53 J. Sun, J. Wan, X. Zhai, J. Wang, Z. Liu, H. Tian and L. Xin, *Toxicol. Ind. Health*, 2021, **37**, 198–209.
54 S. Medici, M. Peana, A. Pelucelli and M. A. Zoroddu, *Semin. Cancer Biol.*, 2021, **76**, 17–26.
55 S. Anees Ahmad, S. Sachi Das, A. Khatoon, M. Tahir Ansari, M. Afzal, M. Saquib Hasnain and A. Kumar Nayak, *Mater. Sci. Energy Technol.*, 2020, **3**, 756–769.
56 L. Marinescu, D. Ficai, O. Oprea, A. Marin, A. Ficai, E. Andronescu and A.-M. Holban, *J. Nanomater.*, 2020, **2020**, 1–14.
57 S. Kumar-Krishnan, A. Hernandez-Rangel, U. Pal, O. Ceballos-Sanchez, F. J. Flores-Ruiz, E. Prokhorov, O. Arias de Fuentes, R. Esparza and M. Meyyappan, *J. Mater. Chem. B*, 2016, **4**, 2553–2560.
58 C. Li, X. Li, X. Duan, G. Li and J. Wang, *J. Colloid Interface Sci.*, 2014, **436**, 70–76.
59 P. Mohammadi, M. Heravi and M. Daraie, *Sci. Rep.*, 2021, **11**, 17124.
60 M. Massaro, R. Noto and S. Riela, *Catalysts*, 2022, **12**, 149.
61 S. Kumar-Krishnan, E. Prokhorov, M. Hernández-Iturriaga, J. D. Mota-Morales, M. Vázquez-Lepe, Y. Kovalenko, I. C. Sanchez and G. Luna-Bárcenas, *Eur. Polym. J.*, 2015, **67**, 242–251.
62 D. Rawtani, Y. K. Agrawal and P. Prajapati, *Bionanoscience*, 2013, **3**, 73–78.
63 A. V. Kornilova, M. V. Gorbachevskii, G. A. Kuralbayeva, S. Jana, A. A. Novikov, A. A. Eliseev, A. N. Vasiliev and V. Y. Timoshenko, *Phys. Status Solidi*, 2019, **216**, 1–5.
64 Q. Zhao, J. Hou, J. Shen, J. Liu and Y. Zhang, *J. Mater. Chem. A*, 2015, **3**, 18696–18705.
65 Y. Chen, Y. Zhang, H. Zhang, J. Liu and C. Song, *Chem. Eng. J.*, 2013, **228**, 12–20.
66 J. Zhang, Y. Zhang, Y. Chen, L. Du, B. Zhang, H. Zhang, J. Liu and K. Wang, *Ind. Eng. Chem. Res.*, 2012, **51**, 3081–3090.
67 Y. V. Cherednichenko, V. G. Evtugyn, L. R. Nigamatzyanova, F. S. Akhatova, E. V. Rozhina and R. F. Fakhrullin, *Nanotechnol. Russ.*, 2019, **14**, 456–461.
68 L.-F. Wang and J.-W. Rhim, *Appl. Clay Sci.*, 2017, **150**, 138–146.
69 H. Fu, Y. Wang, X. Li and W. Chen, *Compos. Sci. Technol.*, 2016, **126**, 86–93.

70 Z. Shu, Y. Zhang, Q. Yang and H. Yang, *Nanoscale Res. Lett.*, 2017, **12**, 135.
71 S. Jana, A. V. Kondakova, S. N. Shevchenko, E. V. Sheval, K. A. Gonchar, V. Y. Timoshenko and A. N. Vasiliev, *Colloids Surf., B*, 2017, **151**, 249–254.
72 R. Al-Gaashani, Y. Zakaria, I. Gladich, V. Kochkodan and J. Lawler, *Sci. Rep.*, 2022, **12**, 21633.
73 M. Tharmavaram, G. Pandey and D. Rawtani, *Adv. Colloid Interface Sci.*, 2018, **261**, 82–101.
74 M.-H. Ho, P.-Y. Kuo, H.-J. Hsieh, T.-Y. Hsien, L.-T. Hou, J.-Y. Lai and D.-M. Wang, *Biomaterials*, 2004, **25**, 129–138.
75 R. Zhang and P. X. Ma, *J. Biomed. Mater. Res.*, 1999, **44**, 446–455.
76 C. Velasquillo, P. Silva-Bermudez, N. Vázquez, A. Martínez, A. Espadín, J. García-López, A. Medina-Vega, H. Lecona, R. Pichardo-Baena, C. Ibarra and K. Shirai, *J. Biomed. Mater. Res., Part A*, 2017, **105**, 2875–2891.
77 C. K. Choo, X. Y. Kong, T. L. Goh, G. C. Ngoh, B. A. Horri and B. Salamatinia, *Carbohydr. Polym.*, 2016, **138**, 16–26.
78 E. Hernández-Jiménez, R. Del Campo, V. Toledano, M. T. Vallejo-Cremades, A. Muñoz, C. Largo, F. Arnalich, F. García-Rio, C. Cubillos-Zapata and E. López-Collazo, *Biochem. Biophys. Res. Commun.*, 2013, **441**, 947–952.
79 T. Rostamzadeh, M. S. Islam Khan, K. Riche', Y. M. Lvov, A. V. Stavitskaya and J. B. Wiley, *Langmuir*, 2017, **33**, 13051–13059.
80 A. Stavitskaya, C. Shakhbazova, Y. Cherednichenko, L. Nigamatzyanova, G. Fakhrullina, N. Khaertdinov, G. Kuralbayeva, A. Filimonova, V. Vinokurov and R. Fakhrullin, *Clay Miner.*, 2020, **55**, 112–119.
81 Y. B. Matos, R. S. Romanus, M. Torquato, E. H. de Souza, R. L. Villanova, M. Soares and E. R. Viana, *Beilstein J. Nanotechnol.*, 2021, **12**, 798–807.
82 A. A. Novikov, A. R. Sayfutdinova, M. V. Gorbachevskii, S. V. Filatova, A. V. Filimonova, U. P. Rodrigues-Filho, Y. Fu, W. Wang, H. Wang, V. A. Vinokurov and D. G. Shchukin, *ACS Omega*, 2022, **7**, 6728–6736.
83 M. S. Arshad, M. Qaiser, K. Mahmood, M. H. Shoaib, N. Ameer, N. Ramzan, M. Hanif and G. Abbas, *Int. J. Biol. Macromol.*, 2022, **212**, 314–323.
84 S. Ghadirian and S. Karbasi, *Int. J. Biol. Macromol.*, 2023, **233**, 123651.
85 P. Yudaev, Y. Mezhuev and E. Chistyakov, *Gels*, 2022, **8**, 329.
86 Y. Yuan, L. Ding, Y. Chen, G. Chen, T. Zhao and Y. Yu, *Int. J. Biol. Macromol.*, 2022, **194**, 644–653.
87 I. M. Radwan, A. Gitipour, P. M. Potter, D. D. Dionysiou and S. R. Al-Abed, *J. Nanopart. Res.*, 2019, **21**, 155.
88 J. Helmlinger, C. Sengstock, C. Groß-Heitfeld, C. Mayer, T. A. Schildhauer, M. Köller and M. Epple, *RSC Adv.*, 2016, **6**, 18490–18501.
89 A. H. Nobbs, R. J. Lamont and H. F. Jenkinson, *Microbiol. Mol. Biol. Rev.*, 2009, **73**, 407–450.